

Seasonal variability of nitrous oxide concentrations and emissions ~~along the Elbe estuary~~ in a temperate estuary

Gesa Schulz^{1,2}, Tina Sanders², Yoana G. Voynova², Hermann W. Bange³, and Kirstin Dähnke²

¹Institute of Geology, Center for Earth System Research and Sustainability (CEN), University Hamburg, Hamburg, 20146, Germany

²Institute of Carbon Cycles, Helmholtz Centre Hereon, Geesthacht, 21502, Germany

³Marine Biogeochemistry Research Division, GEOMAR Helmholtz Centre for Ocean Research Kiel, Kiel, 24105, Germany

Correspondence to: Gesa Schulz (Gesa.Schulz@hereon.de)

Abstract

Nitrous oxide (N₂O) is a greenhouse gas, with a global warming potential 298 times that of carbon dioxide. Estuaries can be sources of N₂O, but their emission estimates have significant uncertainties due to limited data availability and high spatiotemporal variability. We investigated the spatial and seasonal variability of dissolved N₂O and ~~N₂O~~ emissions along the Elbe ~~e~~Estuary (Germany), a well-mixed temperate estuary with high nutrient loading from agriculture. During nine research cruises ~~done~~ performed between 2017 and 2022, we measured dissolved N₂O concentrations, as well as dissolved nutrients and oxygen concentrations along the estuary and calculated N₂O saturations, flux densities and emissions. We found that the estuary was a year-round source of N₂O, with highest emissions in winter when dissolved inorganic nitrogen (DIN) loads and wind speeds are high. However, in spring and summer, N₂O saturations and emissions did not decrease alongside lower riverine nitrogen loads, suggesting that estuarine in-situ N₂O production is an important source of N₂O. We found intense N₂O production along the Elbe estuary that compensated the effect of decreasing dissolved inorganic nitrogen (DIN) loads since the 1990s. We identified two hot-spots areas of N₂O production-production have been identified in the estuary: the Port of Hamburg, a major port region, and the mesohaline estuary near the estuarine maximum turbidity maximum-zone (MTZ). N₂O production was enhanced by warmer temperatures and was fueled by decomposition of riverine organic matter in the Hamburg Port and by marine organic matter in the MTZ. A comparison with previous measurements in the Elbe Estuary revealed that N₂O saturation did not decrease alongside with DIN concentrations after a significant improvement of water quality in the 1990s that allowed for phytoplankton growth to reestablish in the river and estuary. This effect of phytoplankton growth and the overarching control of organic matter on N₂O production, highlights that eutrophication and agricultural nutrient input can increase N₂O emissions in estuaries. Surprisingly, estuarine N₂O emissions were equally high in winter and summer. In winter, high riverine N₂O concentrations led to high N₂O emissions from the estuary, whereas in summer, estuarine biological N₂O production led to equally high N₂O emissions. Overall, we find that the Elbe estuary is a year-round source of N₂O with estimated annual emissions of 0.24 ± 0.06 Gg yr⁻¹.

1 Introduction

Nitrous oxide (N₂O) is an important atmospheric trace gas that contributes to global warming and stratospheric ozone depletion (WMO, 2018; IPCC, 2021). Estuaries are important regions of nitrogen turnover (Middelburg and Nieuwenhuize, 2000; Crossland et al., 2005; Bouwman et al., 2013), and a potential source of N₂O (Bange, 2006;

39 Barnes and Upstill-Goddard, 2011; Murray et al., 2015). Together with coastal wetlands, estuaries contribute
40 between 0.17 and 0.95 Tg N₂O-N of the annual global budget of 16.9 Tg N₂O-N (Murray et al., 2015; Tian et al.,
41 2020). N₂O emission estimates from estuaries are associated with significant uncertainties due to limited data
42 availability and high spatiotemporal variability (e.g. Bange, 2006; Barnes and Upstill-Goddard, 2011; Maavara et
43 al., 2019), presenting a big challenge for the global N₂O emission estimates.

44 Nitrification and denitrification are the most important N₂O production pathways in estuaries. Under oxic
45 conditions, N₂O is produced as a side product during the first step of nitrification, the oxidation of ammonia to
46 nitrite (e.g. Wrage et al., 2001; Barnes and Upstill-Goddard, 2011). At low oxygen (but not anoxic) conditions,
47 nitrifier-denitrification may occur, during which nitrifiers reduce nitrite to N₂O (e.g. Wrage et al., 2001; Bange,
48 2008). Denitrification takes place under anoxic conditions and mostly acts as a source of N₂O, but can also reduce
49 N₂O to N₂ (e.g. Knowles, 1982; Bange, 2008). In estuaries, denitrification ~~mainly can~~ occurs in anoxic sediments,
50 the anoxic water column or anoxic microsites of particles, whereas ~~oxie~~-nitrification and nitrifier-denitrification
51 take place in the oxygenated water column (Beaulieu et al., 2010; Murray et al., 2015; Ji et al., 2018; Tang et al.,
52 2022).

53 In estuaries, the most important factor controlling N₂O emissions are considered to be oxygen availability and
54 dissolved inorganic nitrogen loads (Murray et al., 2015). ~~Beside oxygen availability, temperature, substrate~~
55 ~~availability, pH and water level can also control nitrous oxide production~~ (Murray et al., 2015; Quick et al., 2019)
56 Since N₂O measurements in estuaries are scarce, global N₂O emissions can be estimated by using emission factors
57 and considering dissolved inorganic nitrogen (DIN) or total nitrogen (TN) loads, where it is assumed that higher
58 loads lead to higher N₂O emissions (Kroeze et al., 2005, 2010; Ivens et al., 2011; Hu et al., 2016). However, several
59 studies instead reported no obvious relationship between nitrogen concentrations and N₂O emissions (Borges et
60 al., 2015; Marzadri et al., 2017; Wells et al., 2018), highlighting the need to understand the causes for variability
61 of the relationship between nitrogen loads and N₂O emissions. (Wells et al., 2018).-

62 The Elbe ~~E~~estuary is a heavily managed estuary with high agricultural nitrogen inputs that hosts the third ~~biggest~~
63 ~~largest~~ port in Europe (e.g. Radach and Pätsch, 2007; Bergemann and Gaumert, 2008; Pätsch et al., 2010; Quiel et
64 al., 2011). It has been identified as a N₂O source, with a hotspot of N₂O production in the Port of Hamburg (Hanke
65 and Knauth, 1990; Brase et al., 2017). We aimed to investigate drivers for N₂O emissions along the estuary,
66 specifically the N₂O and DIN ratio (N₂O:DIN). ~~However, the seasonal variability of N₂O along the estuary is~~
67 ~~largely unknown so far~~ To do so, we objectives study were (1) to detect a looked for potential long-term trend
68 changes in of N₂O concentrations saturations, (2) to decipher the investigated potential production hotspots as well
69 as the spatial and temporal distribution of N₂O concentrations saturations along the Elbe estuary during different
70 seasons, and (3) to identify hotspots and drivers for N₂O production and (3) used the N₂O:DIN ratio for a
71 comparison with other estuaries that receive similar high agricultural nutrient inputs. ~~To this end, we present here~~
72 ~~measurements of dissolved N₂O as well as dissolved nutrients and oxygen from nine research cruises along the~~
73 ~~Elbe estuary from August 2017 to March 2022.~~

74 2 Methods

75 2.1 Study site

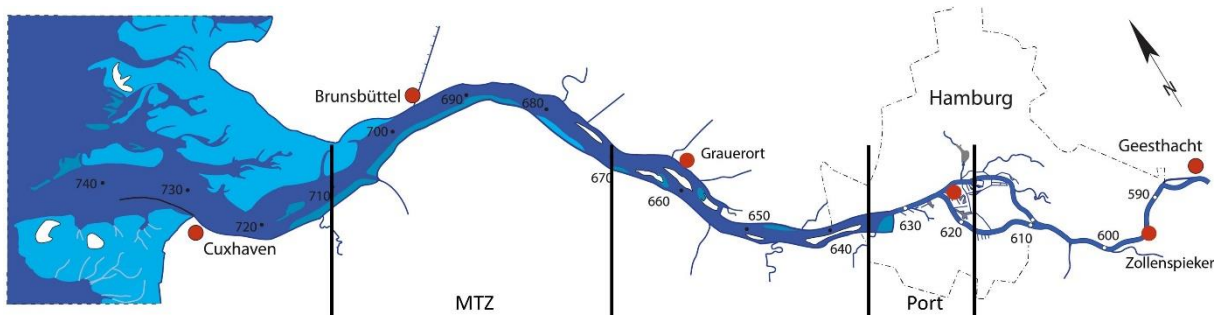
76 The Elbe River stretches over 1094 km from ~~its spring in~~ the Giant Mountains (Czech Republic) to the North Sea
77 (Cuxhaven, Germany). The catchment of the Elbe ~~R~~river is 140 268 km² (Boehlich and Strotmann, 2019), with

78 74 % urban and agricultural land-use (Johannsen et al., 2008). ~~This makes the~~ The Elbe is the second largest German
 79 river discharging into the North Sea, as well as the largest source of dissolved nitrogen for the German Bight,
 80 which is heavily affected by eutrophication (van Beusekom et al., 2019).

81 The Elbe Eestuary is a well-mixed temperate estuary, which begins at stream kilometer 586 at a weir in Geesthacht
 82 and flows-stretches through the Port of Hamburg, entering the North Sea near Cuxhaven at, stream kilometer 727
 83 (Fig. 1). Estuaries are commonly structured along their salinity gradient into an oligohaline section- (salinity: 0.5 –
 84 5.0), a mesohaline section- (salinity: 5.0 – 18.0) and polyhaline section- (salinity > 18.0) (US EPA, 2006). The Elbe
 85 Eestuary has a length of 142 km (Boehlich and Strotmann, 2019) and a mean annual discharge of 712 m³ s⁻¹
 86 (measured at gauge Neu Darchau at stream kilometer 536; of 712 m³ s⁻¹ with a mean variation range of 276 m³ s⁻¹
 87 to 1960 m³ s⁻¹ (measured at gauge Neu Darchau at stream kilometer 536)) (HPA and Freie und Hansestadt Hamburg,
 88 2017). The average water residence time is ~32 days, and-ranges from ~72 days during times of low discharge
 89 (300 m³ s⁻¹) to ~10 days with- during times of high discharge (2000 m³ s⁻¹; Boehlich and Strotmann, 2008). The
 90 estuary has an annual nitrogen load of 84 Gg-N (FGG Elbe, 2018). Point sources along the estuary provide only
 91 small part of the total nitrogen input to the Elbe Estuary (Hofmann et al., 2005; IKSE, 2018). Oxygen
 92 concentrations in the Elbe eEstuary-shows a high seasonal variability vary seasonally, with oxygen depletion
 93 during the summer months and oxygen minimum zones regularly experiencing concentrations below
 94 94 μmol O₂ L⁻¹ In summer months, oxygen depletion and low oxygen zones occur regularly reaching
 95 concentrations below 3 mg O₂ L⁻¹ (Schroeder, 1997; Gaumert and Bergemann, 2007; Schöl et al., 2014).

96 The Elbe Eestuary is dredged year-round-on-a-regular to maintain a water depth of 15 – 20 m and to grant access
 97 for large container ships to the Port of Hamburg (Boehlich and Strotmann, 2019; Hein et al., 2021), which is the
 98 third biggest largest port in Europe (HAFEN HAMBURG, 2021). Construction work for further deepening of the
 99 fairway was carried out in during our study period, from 2019 to early 2022. Upstream of the Port of Hamburg
 100 water depth is less than 10 m (Hein et al., 2021).





102 **Figure 1: Map of the Elbe estuary sampled during the research cruises with stream kilometers indicated (wsv.de, last**
 103 **access: 12.09.2022). Background map: © OpenStreetMap contributors 2021. Distributed under the Open Data 87**
 104 **Commons Open Database License (ODbL) v1.0. The Hamburg Port region stretches from stream kilometer 620—635**
 105 **and is shown between the two grey dashed lines. The typical position of the maximum turbidity zone (MTZ) is shown**
 106 **between the dotted grey lines (Bergemann, 2004).**
 107

108
 109 **Figure 1: Map of the Elbe Estuary sampled during our research cruises with stream kilometers. The vertical black lines**
 110 **indicate the Hamburg Port region and a typical position for the maximum turbidity zone (MTZ, (Bergemann, 2004).**

111 2.2 Transect sampling and measurements

112 We performed nine sampling campaigns along the estuary with the research vessel *Ludwig Prandtl* (Tab-le 1).
 113 Most of the cruises took place during the spring and summer seasons, with water temperatures > 10 °C (May to—
 114 September), while two cruises were conducted in during colder winter months (early March, water temperature <
 115 6 °C;) (Tab-le 1). Transects sampling started in the German Bight, close to the island Scharhörn and continued
 116 along the salinity gradient, through the Port of Hamburg to Oortkaten (stream kilometer 609). To ensure
 117 comparable current and mixing conditions, Ttransect sampling always was performed always done after high-tide,
 118 steaming with the ship travelling upstream against the outgoing tide. For comparison to previous measurements,
 119 we included summer data from a previous study in 2015 (Brase et al., 2017).

120 Table 1: Campaign dates with the sampled Elbe estuary sections shown via stream kilometers, average discharge
 121 during each cruise measured at the Pegel-Neu Darchau gauging station, averages and standard deviations for water
 122 temperature (°C), wind speed (m^3s^{-1}) in at 10 m height, dissolved inorganic nitrogen (DIN) concentrations ($\mu\text{mol L}^{-1}$)
 123 for each campaign.

Campaign Dates	Stream kilometers (km)	Water temperature (°C)	Wind speed 10 m (m s^{-1})	Average discharge ($\text{m}^3\text{ s}^{-1}$)	Average DIN load ($\mu\text{mol L}^{-1}$)
28.-29.04.2015	627 – 741	12.3 ± 1.0	11.8 ± 0.3 <u>7.4 ± 2.3</u>	595	191.0 ± 45.0
02.-04.06.2015	609 – 739	17.4 ± 1.7	5.0 ± 1.3	276	105.9 ± 36.2
01.-02.08.2017	621 – 749	20.9 ± 0.7	3.6 ± 1.5	607	79.2 ± 30.2
04.-05.06.2019	610 – 750	18.7 ± 2.2	4.0 ± 1.7	423	108.3 ± 35.9
30.07.-01.08.2019	609 – 752	22.6 ± 1.0	4.2 ± 1.4	171	60.8 ± 38.6
19.-20.06.2020	609 – 747	19.8 ± 1.4	5.8 ± 1.2	331	74.6 ± 33.8
09.-11.09.2020	607 – 745	18.9 ± 0.6	5.9 ± 2.8	305	93.1 ± 32.7
10.-12.03.2021	609 – 748	5.4 ± 0.5	9.3 ± 2.6	862	324.4 ± 83.8
04.-05.05.2021	610 – 751	10.5 ± 0.8	11.0 ± 3.1	411	85.7 ± 36.6
27.-28.07.2021	621 – 751	22.2 ± 0.7	5.2 ± 1.3	721	139.8 ± 58.4
01.-02.03.2022	610 – 752	5.6 ± 0.2	2.9 ± 1.0	1282	238.0 ± 74.7

124 An onboard membrane pump continuously provided water ~~from at~~ 1.2 m depth to an on-line in-situ FerryBox
 125 system and to an equilibrator used for the measurements of N₂O dry mole fraction (Section 2.4). The FerryBox
 126 system continuously measured water temperature, salinity, oxygen concentrations, pH and turbidity. We corrected
 127 the ~~oxygen measurements using the~~ salinity corrected optode measurements ~~using in~~ comparisons to Winkler
 128 titrations ~~of distinct samples. The corrections of the individual cruises are listed in the~~ See Table S1 ~~for further~~
 129 ~~details.~~

130 Discrete water samples (30-40 samples for each cruise) were ~~taken~~ collected every 20 min from a bypass of the
 131 FerryBox system. For nutrient analysis, water samples were filtered immediately through combusted,
 132 pre-weighted GF/F Filters (4 h, 450 °C), and ~~were stored~~ frozen in acid washed PE-bottles until analysis. The
 133 filters were also stored frozen (-20 °C) and subsequently analyzed for ~~used for the later analysis of~~ suspended
 134 particulate matter (SPM), particulate nitrogen ~~fraction~~-(PN), particulate carbon ~~fraction~~-(PC) and C/N ratios
 135 (~~supplementary material~~ Fig. S1).

136 2.3 Nutrient measurements

137 Filtered water samples were measured in triplicates with a continuous flow auto analyzer (AA3, SEAL Analytics)
 138 using standard colorimetric and fluorometric ~~techniques methods~~ (Hansen and Koroleff, 1999) for dissolved nitrate
 139 (NO_3^-), nitrite (NO_2^-) and ammonium (NH_4^+) concentrations. Detection limits were 0.05 $\mu\text{mol L}^{-1}$, 0.05 $\mu\text{mol L}^{-1}$,
 140 and 0.07 $\mu\text{mol L}^{-1}$ for nitrate, nitrite and ammonium, respectively.

141

142 2.4 Equilibrator based N₂O measurements and calculations

143 Equilibrated dry mole fractions of N₂O were measured by an N₂O analyzer based on off-axis integrated cavity
144 output (OA-ICOS) absorption spectroscopy (Model 914-0022, Los Gatos Res. Inc., San Jose, CA, USA), which
145 was coupled with a sea water/gas equilibrator using off-axis cavity output spectroscopy. Brase et al. (2017)
146 described the set-up and instrument precision in detail. Twice a day, two standard gas mixtures of N₂O in synthetic
147 air (500.5 ppb ± 5 % and 321.2 ppb ± 3 %) were analyzed to validate our measurements. No drift was detected
148 during our cruises.

149 We calculated the dissolved N₂O concentrations in water with the Bunsen solubility function of Weiss and Price
150 (1980), using 1 min averages of the measured N₂O dry mole fraction (ppb). Temperature differences between the
151 sample inlet and the equilibrator were taken into account for the calculation of the final N₂O concentrations Rhee
152 et al. (2009). N₂O saturation were calculated based on N₂O concentrations in water (N₂O_{cw}) and the in the
153 air atmospheric equilibration concentrations (N₂O_{eqair}) (Eq. 1). ~~During each cruise, AA~~ atmospheric N₂O dry mole
154 fractions were measured before and after each transect cruises using an air duct from the deck of the research
155 vessel.

$$s = 100 \times \frac{N_2O_{cw}}{N_2O_{eqair}} \quad (1)$$

156
157 The gas transfer coefficients (k) were determined based on Borges et al. (2004, Eq. 3), ~~(Nightingale et al., (2000),~~
158 ~~(Wanninkhof, (1992) and (Clark et al., (1995), using – taking~~ the Schmidt number (Sc) and wind speeds (u₁₀)
159 measured at in 10-m height (u₁₀) into account (Eq. 2). The Schmidt number was calculated as ratio of the kinematic
160 viscosity in water (Siedler and Peters, 1986) to the N₂O diffusivity in water (Rhee, 2000). ~~Wind speeds were~~
161 ~~measured on board in 10-m height of the R/V Ludwig Prandtl by a MaxiMet GMX600 (Gill Instruments~~
162 ~~Limited). Cruise wind speeds (Table 1) varied significantly from average annual wind speeds of the two federal~~
163 ~~states, in which the Elbe Estuary is located (4.7 m s⁻¹, Schleswig-Holstein u. Hamburg: Mittlere~~
164 ~~Windgeschwindigkeit (1986-2015)* | Norddeutscher Klimamonitor, 2023), and also compared to seasonal average~~
165 ~~wind speeds determined for the stations Cuxhaven and Hamburg (Rosenhagen et al., 2011). Thus, to estimate~~
166 ~~uncertainties due to varying wind conditions during our cruises, we used 1) the in-situ wind speeds measured on~~
167 ~~board the R/V Ludwig Prandtl at 10 m height by a MaxiMet GMX600 (Gill Instruments Limited, Hampshire, UK),~~
168 ~~2) the average annual wind speed (Schleswig-Holstein u. Hamburg: Mittlere Windgeschwindigkeit (1986-2015)*~~
169 ~~| Norddeutscher Klimamonitor, 2023), and 3) the seasonally averaged wind speeds (Rosenhagen et al., 2011). Flux~~
170 ~~densities were calculated according to Equation 3. The flux densities in the main text were calculated using Eq. 3~~
171 ~~and the wind speeds measured on board the vessel. Results of the other calculations are listed in the supplementary~~
172 ~~material (Table S2).~~

$$k = 0.24 \times (4.045 + 2.58u_{10}) \times \left(\frac{Sc}{600}\right)^{-0.5} \quad (2)$$

$$f = k \times (N_2O_{cw} - N_2O_{air}) \quad (3)$$

173 ~~For emission calculations we used an area of 371.85 km² for the Elbe estuary in line with Brase et al. (2017). We~~
174 ~~calculated seasonal averages for winter and spring/summer based on our transect cruises, which we used for~~
175 ~~estimation of annual emissions.~~

176 ~~To estimate N₂O emissions, we separated the Elbe Estuary into five regions: limnic (stream kilometer 585 to 615),~~
177 ~~Port of Hamburg (stream kilometer 615 to 632), oligohaline (stream kilometer 632 to 704), mesohaline (stream~~

178 kilometer 704 – 727) and polyhaline (stream kilometer 727 to 750), see Table S3. Respective areas were provided
179 by the German Federal Waterways Engineering and Research Institute (BAW, pers. Comm., Ortiz, 2023) and
180 (Geerts et al., (2012)). In order to account for seasonality, cruises were defined as: winter (March), spring (April
181 and May), summer (June and July) and late summer/autumn (August and September). We then- calculated daily
182 N₂O emissions per section and season. For upscaling, we used calculated monthly emissions to estimate annual
183 emissions (winter: November to March, spring: April to May, summer: June to July and late summer/autumn:
184 August to October). To address uncertainties, we calculated N₂O emissions based on different parametrizations
185 and wind speeds as described above.

186 2.5 Excess N₂O and apparent oxygen utilization

187 The correlation between excess N₂O (N₂O_{xs}) and apparent oxygen utilization (AOU) can provide insights into N₂O
188 production (Nevison et al., 2003; Walter et al., 2004). We calculated N₂O_{xs} as the difference between the N₂O
189 concentration in water (N₂O_w) and the theoretical equilibrium concentration (N₂O_{eq}) (Eq. 4). AOU was determined
190 using Eq. equation 5, where O₂ is the measured dissolved oxygen concentration, and O₂' is the theoretical
191 equilibrium concentration between water and atmosphere calculated according to Weiss (1970).

$$N_2O_{xs} = N_2O_w - N_2O_{eq} \quad (44)$$

$$AOU = O_2' - O_2 \quad (55)$$

192 A linear relationship between AOU and N₂O_{xs} is usually an indicator for nitrification (Nevison et al., 2003; Walter
193 et al., 2004).

194 2.6 Statistical analysis

195 All statistical analyses were done using R packages. The packages `ggpubr v.0.6.0` (Kassambara, 2023) and `stats`
196 `v.4.0.2` (The R Stats Package, Version 4.0.2, 2021) were used to calculate Pearson correlations (R) and p-values.
197

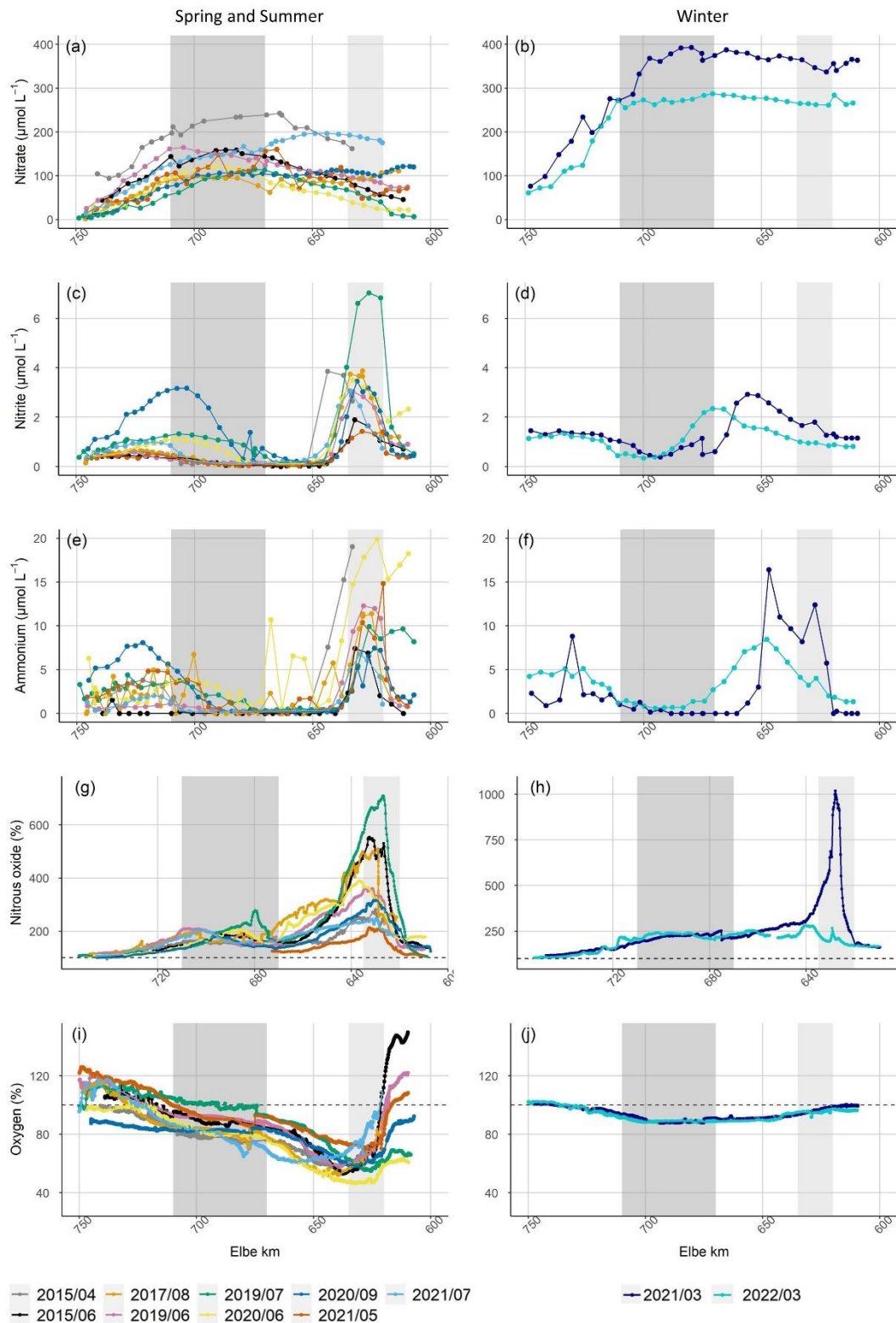
198 3 Results

199 3.1 Hydrographic properties and DIN distribution

200 Discharge ranged between 171 m³ s⁻¹ and 1282 m³ s⁻¹ during our cruises (ZDM, 2022), with higher discharge in
201 winter and lower discharge in summer (Table- 1). Average water temperature over the entire estuary ranged from
202 5.4 ± 0.5 °C in March 2021 to 22.6 ± 1.0 °C in August 2017 (Table- 1). For the further evaluation, March 2021
203 and 2022 cruises ~~will be were~~ regarded as winter cruises (water temperature < 6°C), whereas all cruises with higher
204 water temperature ~~wereare~~ jointly regarded as spring and summer conditions.

205 Nitrate was the major form of dissolved inorganic nitrogen (DIN) during all cruises. In winter, high nitrogen
206 concentrations entered the estuary from the river. Towards summer, the riverine input of nitrate (stream kilometer
207 < 620) decreased, but along the estuary nitrate concentrations increased up to approximate -stream kilometer 700,
208 then decreased ~~again~~ towards the North Sea. Nitrate concentrations were highest during both March cruises with
209 averages of 319.0 ± 85.7 μmol L⁻¹ and 230.9 ± 76.2 μmol L⁻¹ in 2021 and 2022, respectively. During summer,
210 nitrate concentrations were lower, ~~with. The nitrate concentrations~~ averages ~~were~~ between 151.0 ± 58.1 μmol L⁻¹
211 in May 2021 and 63.3 ± 38.8 μmol L⁻¹ in July 2019 (Fig. 2a and b).

212 Nitrite and ammonium concentrations were usually low ($< 1 \mu\text{mol L}^{-1}$) along throughout the Elbe eEstuary, but
 213 peaked showed peaks in the Hamburg Port region and around stream kilometer 720 (Fig. 2c and 2e). We measured
 214 pronounced variations in nitrite concentrations during most of our cruises, ranging from $> 6.0 \mu\text{mol L}^{-1}$ (July 2019)
 215 to concentrations below the detection limit ($< 0.05 \mu\text{mol L}^{-1}$) (Fig. 2c and d). The highest ammonium concentration
 216 was measured in March 2021 at with $23.5 \mu\text{mol L}^{-1}$. Over large stretches of the estuary, ammonium was below
 217 the detection limit ($< 0.07 \mu\text{mol L}^{-1}$) in winter as well as in spring and summer (Fig. 2e and f).



218

Figure 2: Nitrate concentration in $\mu\text{mol L}^{-1}$ along the Elbe estuary (a) in spring/summer, (b) in winter. Nitrite concentration in $\mu\text{mol L}^{-1}$ along the Elbe estuary (c) in spring/summer and (d) in winter. Ammonium concentration in $\mu\text{mol L}^{-1}$ along the Elbe estuary (e) in spring/summer and (f) in winter. N_2O concentration in % saturation along the Elbe estuary (g) in spring/summer, (h) in winter. Dissolved oxygen in % saturation along the Elbe estuary (i) in spring/summer and (j) in winter. All values/variables are plotted against Elbe stream kilometers (Elbe km). Light grey shading denotes the Hamburg Port region, dark grey shading is shown with light grey background. The typical position of the maximum turbidity zone (MTZ) is shown with a dark grey (Bergemann, 2004). Note the difference in Y-axis scales for the plots of N_2O concentrations (g) and (h). The dashed black lines in (g) and (h), as well as (i) and (j) indicate an oxygen-saturation of 100 % for nitrous oxide and dissolved oxygen, respectively.

3.2 Atmospheric and dissolved N_2O and N_2O saturation

The average atmospheric N_2O dry mole fractions ranged from 325 ppb in June 2015 to 336 ppb in July 2022 (Table 2). The differences between our measurements and the mean monthly N_2O mole fraction measured at the Mace Head atmospheric monitoring station Mace Head (Ireland; Dlugokencky et al., 2022) were always less than 1.5 %, indicating a good agreement with the monitoring data.

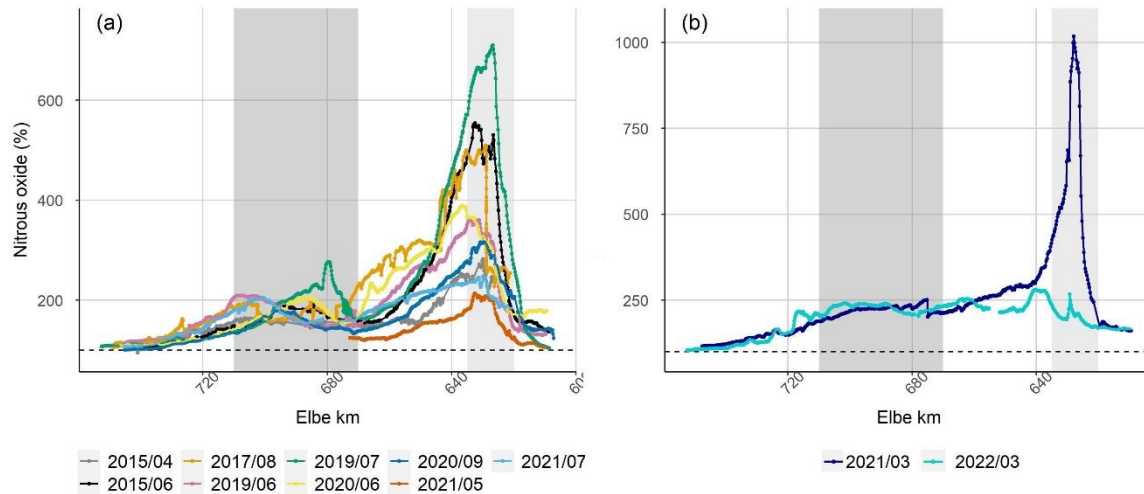
Comparable to the nutrient concentrations, N_2O varied seasonally (Fig. 2): In spring and summer, riverine N_2O (i.e., inflow into the estuary, stream kilometer <589) ranged from 8 nmol L^{-1} to 15 nmol L^{-1} . At the onset of the estuary, spring and summer N_2O concentrations usually showed a steep increase and peak values between 27 nmol L^{-1} and 58 nmol L^{-1} (stream kilometer 620–635). Further downstream, N_2O concentrations decreased towards a local minimum (stream kilometer 670). A second peak was located along the salinity gradient at salinity 5 (stream kilometer 680–700) ranging from 17 nmol L^{-1} to 22 nmol L^{-1} . N_2O concentrations dropped towards equilibrium concentrations of 8–12 nmol L^{-1} in the North Sea (Fig. 2g).

In winter, riverine N_2O concentrations were elevated (25 nmol L^{-1}) compared to spring and summer riverine concentrations. In 2021, a steep increase of N_2O concentrations occurred in the Hamburg Port region, (stream kilometer 620–635) leading to exceptionally elevated N_2O concentrations of up to 158 nmol L^{-1} (Fig. 2h). In March 2022, N_2O increased to 44 nmol L^{-1} in this region. Further downstream, N_2O concentrations remained relatively constant at 35 nmol L^{-1} during both cruises, and dropped to near equilibrium concentrations between stream kilometer 700 and the coastal ocean.

3.3 N_2O saturations and flux densities

During all cruises, the Elbe estuary was supersaturated in N_2O in the freshwater region (Fig. 2g, h). The average N_2O saturation over the entire transect ranged between 146 % and 243 % with an overall average of 197 % for all cruises. Highest N_2O saturations occurred in the Hamburg Port region in spring and summer with an average N_2O peak of 402 % saturation and a maximum supersaturation of 710 % in July 2019. The distributions of N_2O saturations during the winter cruises were significantly different: In March 2022, highest N_2O saturation (280 % saturation) occurred at stream kilometer 640. In contrast, in March 2021, we found an extraordinarily high peak with a saturation of 1018 % at stream kilometer 627. Between stream kilometer 680 and 720, a supersaturation of up to 277 % occurred in spring and summer months. Further towards the North Sea, N_2O saturation decreased, and approaching equilibrium with the atmosphere.

3.4.3.3 N_2O flux densities and N_2O emissions



259 **Figure 3: (a): N₂O saturation along the Elbe estuary for cruises in spring/summer, (b) N₂O saturation for the cruises**
 260 **done in March. The dashed black lines in both plots indicate a saturation of 100 %. The Hamburg Port region is shown**
 261 **with a background in light grey. The typical position of the maximum turbidity zone (MTZ) is shown with a dark grey**
 262 **(Bergemann, 2004). Y-axis scales differ for both plots.**
 263

264 For N₂O flux densities, we in the following present calculated values after Borges et al. (2004, Table 2). See Table
 265 S2 for results of other parametrizations. The N₂O flux densities were usually highest in the Hamburg Port area,
 266 with an average of $95.095.1 \pm 113.697.9 \mu\text{mol m}^{-2} \text{d}^{-1}$ and lowest towards the North Sea, with an average of
 267 $3.9_{-3.0} \mu\text{mol m}^{-2} \text{d}^{-1}$ (Elbe stream kilometers > 735). The average N₂O flux density of all cruises was
 268 $37.839.9 \pm 51.46.90 \mu\text{mol m}^{-2} \text{d}^{-1}$. (Tab. 2 calculated (Borges et al., 2004), with in-situ wind speeds measured
 269 during the cruises).

270 **Table 2: Calculated average N₂O saturation, sea-to-air fluxes calculated following Borges et al. (2004) and atmospheric**
 271 **N₂O dry mole fractions during our cruises infor the Elbe Estuary**

Campaign Dates	Average saturation (%)	N ₂ O Flux densities ($\mu\text{mol m}^{-2} \text{d}^{-1}$)			Average atmospheric dry mole fraction (ppb)
		In-situ wind	Annual wind	Seasonal wind	
28.-29.04.15	160.8 ± 37.9	33.1 ± 21.0	23.1 ± 14.7	25.4 ± 16.1	331 ± 0.5
02.-04.06.15	203.8 ± 112.7	39.0 ± 42.7	37.2 ± 40.7	37.8 ± 41.4	325 ± 0.8
01.-02.08.17	221.0 ± 106.5	35.6 ± 31.8	43.2 ± 38.5	44.1 ± 39.3	331 ± 1.2
04.-05.06.19	192.6 ± 66.0	29.7 ± 21.5	33.5 ± 24.2	34.0 ± 24.6	332 ± 0.2
30.07.-01.08.19	232.5 ± 155.3	42.0 ± 50.1	45.7 ± 54.5	47.4 ± 56.4	327 ± 1.0
19.-20.06.20	193.9 ± 74.1	39.2 ± 31.6	33.3 ± 26.9	33.9 ± 27.3	330 ± 0.6
09.-11.09.20	160.5 ± 53.6	26.0 ± 23.5	21.8 ± 19.7	24.5 ± 22.1	331 ± 0.7
10.-12.03.21	242.5 ± 141.6	100.7 ± 101.2	58.1 ± 58.4	71.0 ± 71.4	331 ± 1.3
04.-05.05.21	145.6 ± 28.8	35.6 ± 22.5	17.8 ± 11.2	18.5 ± 11.7	331 ± 0.8
27.-28.07.21	172.6 ± 37.2	28.0 ± 14.6	25.9 ± 13.6	26.9 ± 14.1	334 ± 3.8
01.-02.03.22	196.5 ± 47.0	27.8 ± 13.9	39.0 ± 19.5	47.7 ± 23.8	333 ± 0.7

272
 273
 274 N₂O emission estimates varied significantly depending on the used parametrization and wind speeds. Note that we
 275 calculated emission twice: 1) including (w 03/2021) and 2) deliberately excluding (w/o 03/2021) the N₂O peak
 276 saturation measured in the Port of Hamburg in March 2021, using a linear interpolated concentrations in the

277 respective. Highest emissions were calculated following methods by Borges et al. (2004) and using in-situ wind
 278 speeds, resulting in emissions of 0.25 ± 0.16 Gg-N₂O yr⁻¹ and 0.23 ± 0.12 Gg-N₂O yr⁻¹ with and without the N₂O
 279 peak in March 2021, respectively. Lowest emissions of 0.08 Gg-N₂O yr⁻¹ arose with parametrization of
 280 (Nightingale et al., (2000) and (Wanninkhof, (1992), and using annual wind speeds (Table 3).

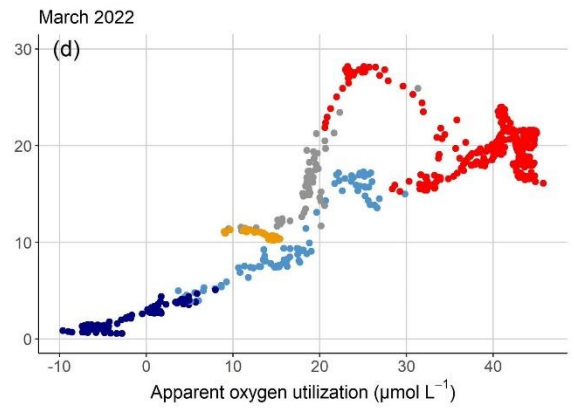
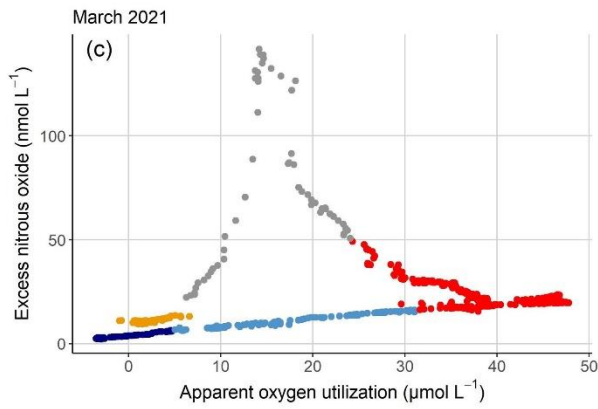
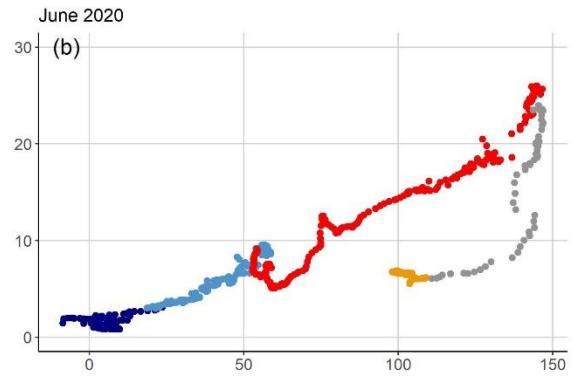
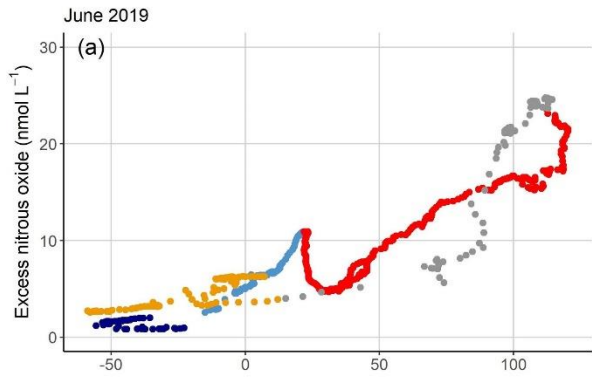
281 **Table 3: Annual N₂O emission estimates in Gg-N₂O yr⁻¹ calculated with different parametrizations and wind speeds**

		Emissions in Gg-N ₂ O yr ⁻¹			
		Borges et al. (2004)	(Nightingale et al., (2000)	(Wanninkhof, (1992)	(Clark et al., (1995)
<u>w</u>	<u>In-situ wind</u>	<u>0.25 ± 0.16</u>	<u>0.14 ± 0.12</u>	<u>0.17 ± 0.15</u>	<u>0.16 ± 0.12</u>
<u>03/2021</u>	<u>Annual wind</u>	<u>0.21 ± 0.11</u>	<u>0.08 ± 0.04</u>	<u>0.09 ± 0.05</u>	<u>0.09 ± 0.05</u>
	<u>Seasonal wind</u>	<u>0.24 ± 0.12</u>	<u>0.11 ± 0.06</u>	<u>0.13 ± 0.06</u>	<u>0.12 ± 0.06</u>
<u>w/o</u>	<u>In-situ wind</u>	<u>0.23 ± 0.12</u>	<u>0.13 ± 0.09</u>	<u>0.15 ± 0.11</u>	<u>0.14 ± 0.09</u>
<u>03/2021</u>	<u>Annual wind</u>	<u>0.20 ± 0.08</u>	<u>0.08 ± 0.03</u>	<u>0.08 ± 0.03</u>	<u>0.09 ± 0.04</u>
	<u>Seasonal wind</u>	<u>0.22 ± 0.09</u>	<u>0.11 ± 0.04</u>	<u>0.12 ± 0.04</u>	<u>0.12 ± 0.04</u>

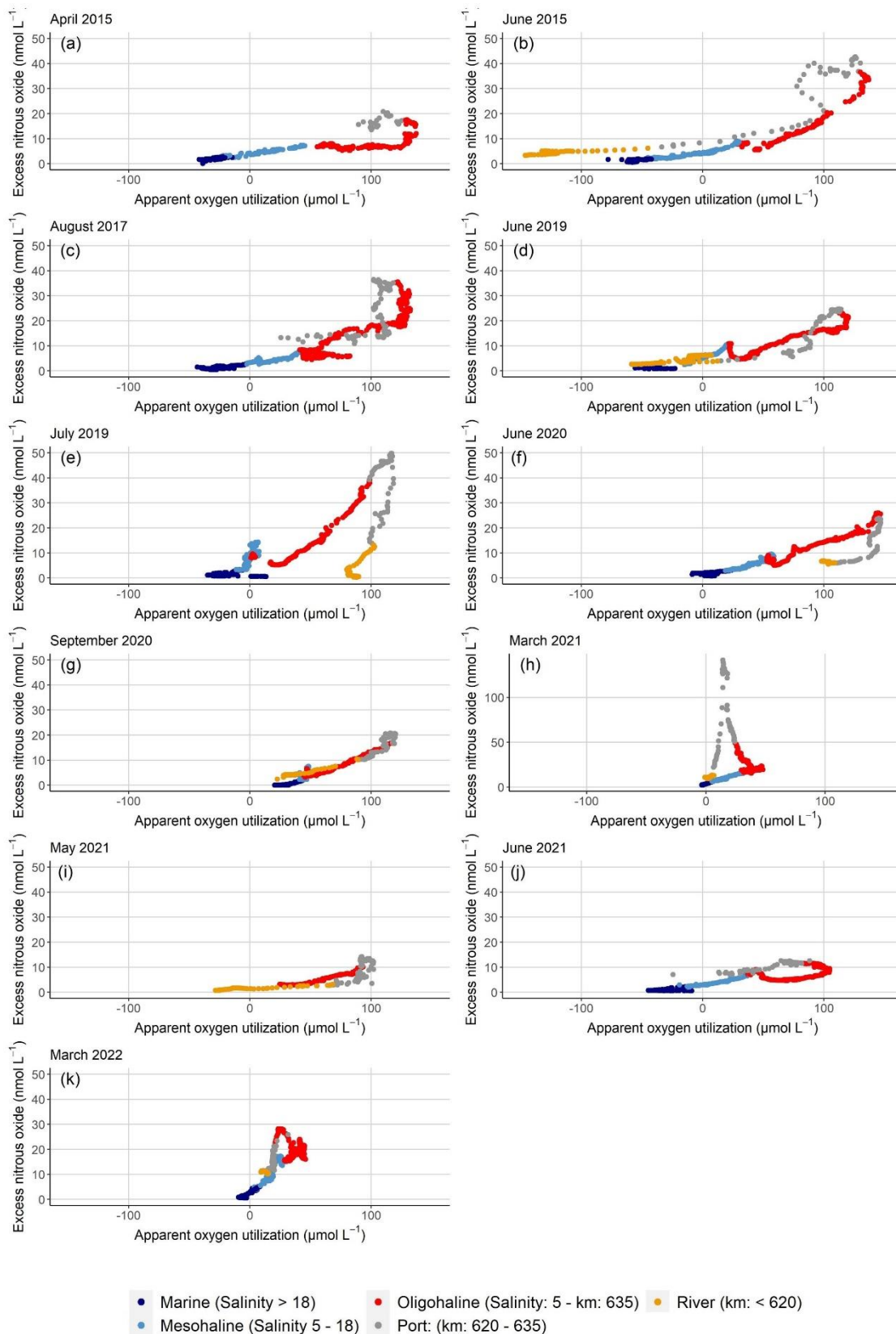
282 3.5.3.4 Dissolved oxygen saturation

283 Average oxygen ~~saturation~~ varied between 76 and 95 ~~in~~-% saturation with an oxygen minimum in the Hamburg
 284 Port area. Winter cruises ~~varied little~~~~showed only little variation~~, with oxygen remaining relatively constant along
 285 the estuary (> 88 % saturation). During most spring and summer cruises, water from the river coming into the
 286 estuary was high-supersaturated in oxygen (> 100 % saturation). In the Hamburg Port region, oxygen saturation
 287 generally decreased. Lowest values occurred in June 2020 with 47 % saturation. The along-estuary oxygen
 288 minimum ~~oxygen~~ in summer months (June ~~to~~- August) was always below 61 % saturation. In spring and summer,
 289 oxygen increased towards the North Sea and reached 100 ~~-%~~-saturation (Fig. 2i and j).

290 Plots of excess N₂O (N₂O_{xs}) and apparent oxygen utilization (AOU) revealed excess N₂O along the entire estuary
 291 (Fig. 3). During all cruises, elevated riverine N₂O_{xs} entered the estuary (stream kilometer < 620). A linear positive
 292 relationship between N₂O_{xs} and AOU suggested nitrification as main production pathway in large sections of the
 293 estuary (Nevison et al., 2003; Walter et al., 2004). However, in summer, a change of slope in the Port of Hamburg
 294 as well as in the mesohaline section of the estuary suggested either increased in-situ N₂O production or external
 295 N₂O input. In winter, we found an increasing slope in the Hamburg Port region and in the oligohaline part of the
 296 Elbe Estuary (Fig. 3h, k).~~Plots of excess N₂O (N₂O_{xs}) and apparent oxygen utilization (AOU) (Fig. 4) revealed~~
 297 ~~excess N₂O along the entire estuary (Fig. 4 and supplementary material S2). During all cruises, elevated riverine~~
 298 ~~N₂O_{xs} concentrations entered the estuary (stream kilometer < 620). In spring and summer, steep, non-linear~~
 299 ~~increases of N₂O_{xs} in the Port of Hamburg suggested in-situ N₂O production (Fig. 4a, 4b). This production extended~~
 300 ~~into the oligohaline estuary (stream kilometer > 635 and salinity < 5) followed by a linear decrease of N₂O_{xs}~~
 301 ~~reduction in the transition region to the mesohaline section of the estuary (salinity: 5-18), N₂O_{xs} increased again,~~
 302 ~~followed by a decrease to 0 nmol L⁻¹ towards the North Sea. In winter, we found a linear relationship of N₂O_{xs} and~~
 303 ~~AOU along the estuary, with a decoupling in the Hamburg Port and the oligohaline part of the Elbe estuary. In~~
 304 ~~Figure 4, representative N₂O_{xs}/AOU plots for summer (4 a, b) and winter (4 c, d) are shown (see supplementary~~
 305 ~~material: Fig. S2 for all plots).~~



- Marine (Salinity > 18)
- Mesohaline (Salinity 5 - 18)
- Oligohaline (Salinity: 5 - km: 635)
- Port: (km: 620 - 635)
- River (km: < 620)



307

308 **Figure 43: Representative pPlots of N_2O_{xs} vs AOU for (a) June 2019, (b) June 2015–June 2020, (c) March 2021, (d) March 2022, (e) June 2019, (f) June 2020, (g) September 2020, (h) March 2021, (i) May 2021, (j) June 2021 and (k) March 2022.** The values are colored to distinguish between different regions of the estuary. Values upstream of stream kilometer 620 are yellow. In the Hamburg Port region (km: 620–635), points are colored grey. Red points mark the region downstream of the port with low salinity (km: 635–salinity 5). Up to stream kilometer 720, points are light blue (mesohaline part, salinity: 5–18) and everything further out in the North Sea is a dark blue (salinity > 18). Y-axis scale differ for Fig. 4e3h.

309
 310
 311
 312
 313
 314

3.5 Statistical analysis

We performed a statistical analyses to identify potential N₂O production pathways and controlling factors. Table 4 summarizes the results for the entire data set with further separation into spring and summer cruises (sp/su), as well as separation according to presence of a salinity gradient (salinity > 1) or freshwater regions (salinity < 1). Further, we performed corresponding analysis to assess the significance of correlations between for average values of different parameters for each cruise (Table 5).

Table 4: Pearson correlation coefficients (R) for N₂O saturation (%) with temperature (T in °C), pH value, oxygen (O₂ in %), ammonium concentrations (NH₄⁺ in μmol L⁻¹), nitrite concentrations (NO₂⁻ in μmol L⁻¹), nitrate concentrations (NO₃⁻ in μmol L⁻¹), SPM concentrations (SPM in mg L⁻¹), C/N values, particulate carbon fraction (PC in %) and particulate nitrogen fraction (PN in %) for the entire data set, spring and summer cruises (sp/su), data with salinity > 1, spring and summer cruises with salinity > 1, data with salinity < 1 and spring and summer cruises with salinity < 1. The significance is shown as ** for p-value < 0.001, * for p-values < 0.01 and + for p-values < 0.05.

N ₂ O saturation %	T °C	pH	O ₂ %	NH ₄ ⁺ μM	NO ₂ ⁻ μM	NO ₃ ⁻ μM	SPM mg	C/N	PC %	PN %
Entire data	0.06	-0.47**	-0.56**	0.27**	0.48**	0.23	0.10	0.60	-0.05	-0.13 ⁺
sp/su	0.33*	-0.59**	-0.65**	0.23**	0.53**	0.09	0.02	0.24**	-0.09	-0.13 ⁺
Sal>1	0.03	-0.40**	-0.53**	-0.32**	-0.05	0.71**	0.32**	0.11*	-0.24	-0.39**
Sal<1	0.01	-0.41**	-0.42**	0.28**	0.51**	-0.00	-0.08	0.15	-0.25*	-0.24*
Sal>1, sp/su	-0.10	-0.21 ⁺	-0.52**	-0.28**	0.01	0.62**	0.02	0.39**	-0.31**	-0.41**
Sal<1, sp/su	0.30**	-0.60**	-0.57**	0.21 ⁺	0.58**	-0.23*	-0.16 ⁺	0.11	-0.30*	-0.27*

Table 5: Pearson correlation coefficients (R) for average N₂O saturation (%) with average discharge (Q in m³ s⁻¹) temperature (T in °C), pH value, oxygen (O₂ in %), ammonium concentrations (NH₄⁺ in μmol L⁻¹), nitrite concentrations (NO₂⁻ in μmol L⁻¹), nitrate concentrations (NO₃⁻ in μmol L⁻¹), SPM concentrations (SPM in mg L⁻¹), C/N values, particulate carbon fraction (PC in %) and particulate nitrogen fraction (PN in %) for the entire data set, spring and summer cruises (sp/su), data with salinity > 1, spring and summer cruises with salinity > 1, data with salinity < 1 and spring and summer cruises with salinity < 1. The significance is shown as ** for p-value < 0.001, * for p-values < 0.01 and + for p-values < 0.05.

N ₂ O saturation %	Q m ³ s ⁻¹	T °C	pH	O ₂ %	NH ₄ ⁺ μM	NO ₂ ⁻ μM	NO ₃ ⁻ μM	SPM mg	C/N	PC %	PN %
Entire data	0.13	0.06	-0.65	-0.39	0.02	0.48	0.27	-0.31	0.53	0.12	-0.16
sp/su	-0.26	0.76 ⁺	-0.82 ⁺	-0.32	0.01	0.35	-0.40	-0.92*	0.15	0.18	0.31
Sal>1	-0.07	-0.14	-0.38	-0.43	-0.18	0.23	0.52	-0.19	0.46	-0.18	-0.38
Sal<1	-0.21	0.29	-0.59	-0.39	0.26	0.76*	-0.11	-0.57	0.12	0.61	0.47
Sal>1, sp/su	-0.07	-0.70 ⁺	-0.41	-0.26	-0.42	0.03	0.05	-0.81 ⁺	-0.04	-0.10	0.14
Sal<1, sp/su	-0.48	0.72 ⁺	-0.80	-0.46	0.29	0.77 ⁺	-0.58	-0.87 ⁺	-0.17	0.69	0.67

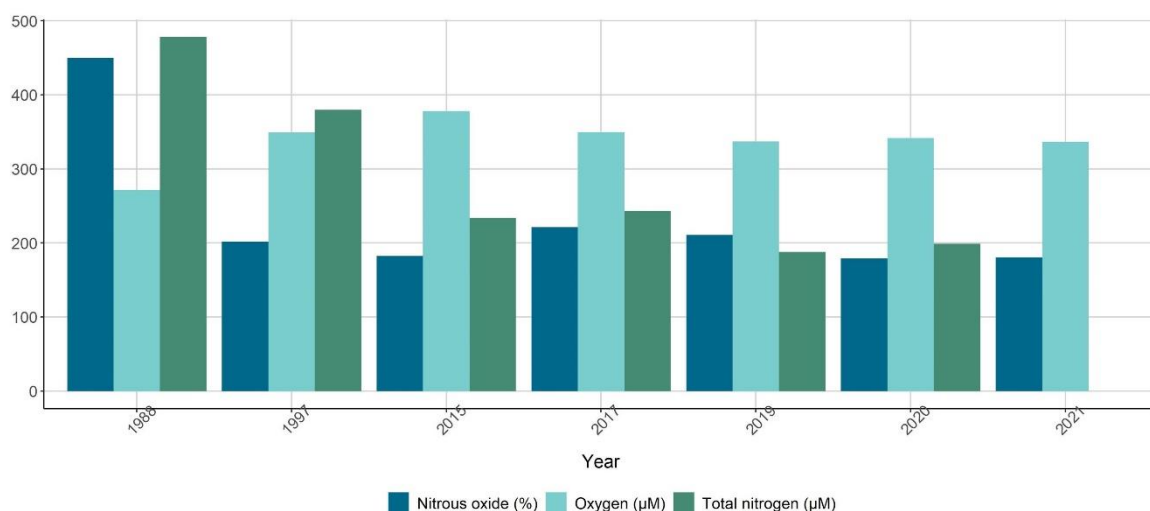
4 Discussion

4.1 N₂O saturation and flux densities of the Elbe Estuary

The average N₂O saturation and flux density were 197 % and 39.9 ± 46.9 ~~39.68~~ μmol m⁻² d⁻¹, respectively. The N₂O flux densities from the Elbe ~~estuary~~ Estuary were in the mid-range of flux densities of other European estuaries ranging from 2.9 μmol m⁻² d⁻¹ to 96.5 μmol m⁻² d⁻¹ (Garnier et al., 2006; Gonçalves et al., 2010; Murray

341 et al., 2015) and average N_2O saturations fitted to values determined by (Reading et al., (2020) for highly modified
 342 urban systems. But they were significantly lower than observed medians for tidal environments with high DIN
 343 loads ($72 \mu\text{mol m}^{-2} \text{d}^{-1}$ and $168 \mu\text{mol m}^{-2} \text{d}^{-1}$) (Murray et al., 2015). As shown in Fig. 4, there was no linear
 344 relationship between N_2O_{xs} and AOU for most of the regions of the Elbe estuary. Therefore, large sections in the
 345 estuary. The relationship of N_2O_{xs} and AOU (Fig. 3), with changing slopes in the Port of Hamburg and mesohaline
 346 estuary, were influenced was determined by either initial riverine N_2O production, or in-situ production along the
 347 estuary. During spring and summer, we found enhanced-increasing N_2O concentrations in two regions: the
 348 Hamburg Port region (see also Brase et al. (2017)), and in the salinity gradient (stream kilometer 680 – 700, salinity
 349 ~5). Both N_2O peaks varied in magnitude height and spatial extension, suggesting in-situ biological production
 350 (Fig. 2g, 3a). This matches previous-earlier research linking estuarine N_2O fluxes to in-situ generation (e.g. Bange,
 351 2006; Barnes and Upstill-Goddard, 2011; Murray et al., 2015).

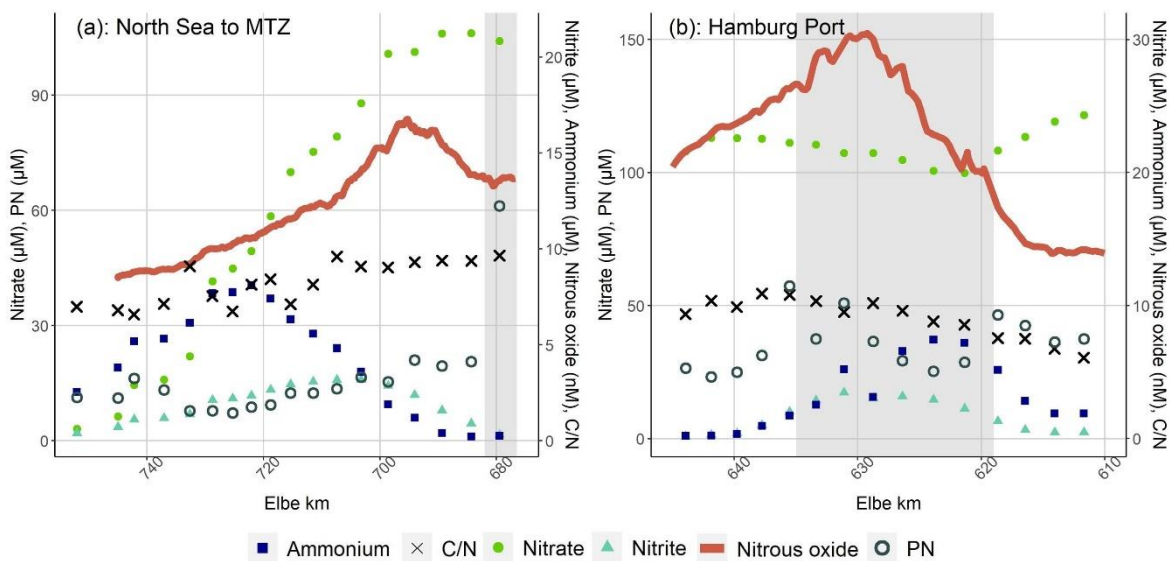
352 Previous measurements of N_2O saturation and flux densities in the Elbe Estuary between the 1980s and 2015
 353 (Hanke and Knauth, 1990; Barnes and Upstill-Goddard, 2011; Brase et al., 2017) showed a significant reduction
 354 of N_2O saturation due to the reduced riverine nutrient load and higher dissolved oxygen concentrations (Brase et
 355 al., 2017). However, since the BIOGEST study in 1997 (Barnes and Upstill-Goddard, 2011), N_2O remained
 356 relatively stable at ~ 200 % saturation despite a concurrent decrease in TN concentration from $\sim 400 \mu\text{mol L}^{-1}$ to
 357 around $200 \mu\text{mol L}^{-1}$ (Fig. S2; Hanke and Knauth, 1990; Barnes and Upstill-Goddard, 2011; Brase et al., 2017;
 358 Das Fachinformationssystem (FIS) der FGG Elbe, 2022). As N_2O saturation did not decrease in scale with riverine
 359 nitrogen input, this suggests suggesting that in-situ N_2O production along the estuary is important (Fig. 5). Dähnke
 360 et al. (2008) showed a shift from dominating denitrification towards significant nitrification in the Elbe Estuary
 361 due to the significant improvement of water quality after the reunification of Germany in 1990. In the following
 362 sections, we investigate the biogeochemical controls of this in-situ production. For this purpose, we discuss both
 363 the two zones of intense N_2O production separately and also distinguish between biological active cruises in spring
 364 and summer (water temperature > 10 °C) and in winter (water temperature < 6 °C).



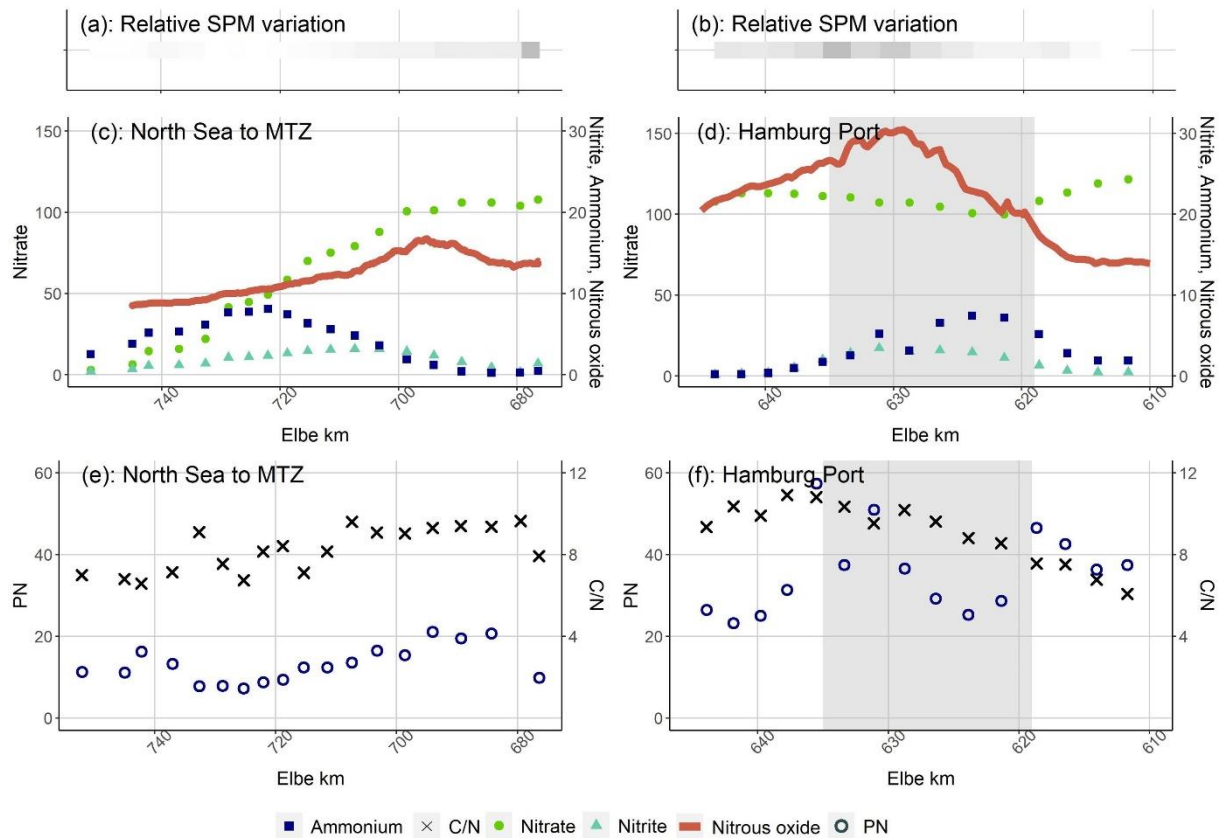
365
 366 **Figure 5: Comparison of average N_2O saturation transect measurements with previous research from the Elbe estuary. Average annual oxygen concentration and total nitrogen concentration are shown for the station Zollenspieker at the beginning of the estuary (stream kilometer 598.7) and publicly available (Das Fachinformationssystem (FIS) der FGG Elbe, 2022). Values for 2022 and total nitrogen concentration for 2021 are not presented as the data is not publicly available yet.**
 368
 369
 370

371 **4.2 N₂O production in spring and summer in the mesohaline estuary**

372 The N₂O peak in the transition between oligohaline and mesohaline estuary was accompanied by a sudden change
 373 ~~from a decreasing to an increasing trend between in the slope of the AOU and vs N₂O_{xs} plots~~ (Fig. 4a, 4b3), pointing
 374 towards N₂O production in the oxic water column. ~~Interestingly, we find that small peaks~~ Peaks of nitrite and
 375 ammonium ~~concentrations~~ coincided with the ~~elevated~~ nitrous oxide ~~saturation peak~~ between Elbe km 680–700,
 376 with ~~an~~ ammonium ~~peak~~ around stream kilometer ~720, and a nitrite peak at ~700 (Fig. 4a). Highest N₂O
 377 concentrations were usually measured between the nitrite peak and the region with highest turbidity ~~(see Fig. 6 for~~
 378 ~~an example, supplementary material Fig. S3-S13), as seen for our cruise in September 2020 in~~ (Fig. 6a4a,
 379 ~~September 2020, and Fig. S3-S13). This co-occurrence of nitrite accumulation and increased N₂O saturation has~~
 380 ~~been interpreted as signs for N₂O production via denitrification~~ (e.g. Wertz et al., 2018; Sharma et al., 2022).
 381 ~~However, denitrification does not seem likely in this oxic water column.~~ Such a succession of nitrite and
 382 ammonium peaks is ~~also~~ typical for remineralization and nitrification, and the slight decrease of oxygen
 383 concentrations around the ~~higher~~ N₂O ~~saturation peak~~ (Fig. 2g and i) suggests ~~that~~ oxygen consumption, possibly
 384 caused by ~~nitrification these two processes, occurred~~. Sanders et al. (2018) measured small but detectable
 385 nitrification rates (~~of~~ 1 – 2 μmol L⁻¹ d⁻¹) for this region of the Elbe ~~E~~ estuary, suggesting that N₂O ~~in this region~~
 386 may be a side product of nitrification.



387



388

389 **Figure 64: (a) Succession of N-bearing substances coming from the North Sea and in the Port of Hamburg in September**
 390 **2020: Relative change of SPM concentrations (a) from the North Sea and (b) in the Port of Hamburg. Nitrate in**
 391 **$\mu\text{mol L}^{-1}$, nitrite in $\mu\text{mol L}^{-1}$, ammonium in $\mu\text{mol L}^{-1}$ and nitrous oxide concentrations in nmol L^{-1} plotted against Elbe**
 392 **stream kilometers (c) from the North Sea and (d) in the Port of Hamburg. Particulate nitrogen concentrations in**
 393 **$\mu\text{mol L}^{-1}$ and C/N values plotted against stream kilometers (e) from the North Sea and (f) in the Port of Hamburg. The**
 394 **grey area in (f) and (f) shows the position of the MTZ/Port of Hamburg. (b)**

395 **Succession of N-bearing substances in the Port of Hamburg in September 2020. The grey area shows the position of the**
 396 **Port of Hamburg. On the left y-axis nitrate concentrations in $\mu\text{mol L}^{-1}$ are presented as green circles and particulate**
 397 **nitrogen (PN) concentrations as unfilled circles in $\mu\text{mol L}^{-1}$. The right y-axis shows nitrite concentrations in $\mu\text{mol L}^{-1}$ as**
 398 **light blue triangles, ammonium concentration in $\mu\text{mol L}^{-1}$ as dark blue squares, nitrous oxide concentration in nmol L^{-1}**
 399 **as a red line and C/N ratios as grey crosses.**

400 However, this suggests input of particulate matter from the North Sea and upstream particle transport towards
 401 the maximum turbidity zone of the estuary (MTZ). This transport mechanism is in line with Wolfstein and Kies
 402 (1999), who explained organic matter contents and chlorophyll a concentrations in the polyhaline part of the Elbe
 403 estuary by input of freshly produced marine particulate matter of marine origin. Generally, the occurrence of an
 404 MTZ is unique to each estuary and its maximum turbidity zones are generated by the balance between river-induced
 405 flushing and upstream transport of marine SPM, as well as a function of estuarine geomorphology, gravitational
 406 circulation and tidal flow, trapping the particles in the MTZ (Bianchi, 2007; Sommerfield and Wong, 2011;
 407 Winterwerp and Wang, 2013). Other studies detected N_2O production from water column nitrification in estuarine
 408 MTZs (e.g. Barnes and Owens, 1999; de Wilde and de Bie, 2000; Bange, 2006; Barnes and Upstill-Goddard, 2011;
 409 Harley et al., 2015), caused by high bacterial numbers, particulate nitrogen availability and long residence times
 410 (Murray et al., 2015).

411 For the selected dataset, we calculated a negative correlation between average SPM concentrations and N_2O
 412 saturation ($R = -0.81$, Table 5), and found that the N_2O peak was located downstream of the MTZ, and upstream
 413 of increasing nitrite and ammonium concentrations (Fig. 64a). This (+) suggests that (1) the mere concentration of
 414 SPM is not the driving factor of nitrification as a source of N_2O , but that organic matter quality is key to biological

415 turnover (Dähnke et al. 2022), and (2) ~~speaks in favor of~~ material transport from the North Sea upstream towards
416 the MTZ (Kappenberg and Fanger, 2007; Schoer, 1990) is a main mechanism for N₂O generation ~~(?)~~ (Kappenberg
417 and Fanger, 2007; Schoer, 1990). We find organic matter with low C/N ratios, and with relatively high PN and PC
418 contents in the outermost samples (ranging from 5.9 in June 2020 to 8.8 August 2017), indicating fresh and easily
419 degradable organic matter (supplementary material Fig. S1, e.g. Redfield et al. 1963; Fraga et al. 1998; Middelburg
420 and Herman 2007). Towards the MTZ, C/N values, PN and PC contents decreased, indicating remineralization in
421 the water column. This remineralization and subsequent nitrification can then cause the observed succession of
422 ammonium, nitrite and N₂O peaks (Fig. 4a6), contributing to the ~~already~~ high nitrate concentrations in the MTZ
423 ~~coming from the upper estuary~~, where high C/N values (9 – 11/16) indicate low organic matter quality (e.g.
424 Hedges and Keil 1995; Middelburg and Herman 2007).

425 Overall, we conclude that remineralization of marine organic matter, followed by nitrification, produced the N₂O
426 peak in the salinity gradient of the Elbe ~~estuary~~ Estuary. This production was mainly fueled by fresh organic matter
427 entering the estuary from the North Sea.

428 4.3 Hamburg Port: N₂O production in spring and summer

429 ~~Several studies identified the Hamburg Port region as a hotspot of biogeochemical turnover: Deek et al. (2013)~~
430 ~~showed ongoing denitrification, Sanders et al. (2018) measured intense nitrification, Norbistrath et al. (2022)~~
431 ~~determined intense total alkalinity generation, and Dähnke et al. (2022) found that nitrogen turnover were driven~~
432 ~~by particulate organic matter. The highest N₂O peaks of our study were located in the Port of Hamburg. Brase et~~
433 ~~al. (2017) identified the port region as a hotspot of N₂O production and hypothesized that simultaneous nitrification~~
434 ~~and denitrification were responsible. We use our expanded dataset to further evaluate this hypothesis. During all~~
435 ~~cruises, we measured highest N₂O saturation in the Port of Hamburg. These peaks can be caused by input from a~~
436 ~~waste water treatment plant, by deepening and dredging operations, enhanced benthic production or by in-situ~~
437 ~~production in the water column.~~

438 ~~Point sources generally play a minor role in the Elbe Estuary (Hofmann et al., 2005; IKSE, 2018). We estimated~~
439 ~~the wastewater discharge fraction of stream flow according to Büttner et al. (2020) for the waste water treatment~~
440 ~~plant (WWTP) Köhlbrandhöft, which treats the waste water from the Hamburg metropolitan region, with less than~~
441 ~~5 % even under low fresh water inflow. Thus, point sources seemed not to be the cause for the elevated N₂O~~
442 ~~concentrations.~~

443 ~~Dredging can be a potential source of N₂O in the water column. The estuary is continuously deepened and dredged~~
444 ~~to grant access for large container ships, which stirs up bottom sediments. Ammonium concentrations in the~~
445 ~~sediment pore water are high (Zander et al., 2020, 2022) and N₂O can be produced by nitrifier-denitrification in~~
446 ~~the sediments (Deek et al., 2013). However, we found no correlation of high SPM concentrations and N₂O~~
447 ~~saturation, indicating no major influence on N₂O dynamics from channel dredging and deepening.~~

448 ~~Several studies identified the Hamburg Port region as a hotspot of biogeochemical turnover: Deek et al. (2013)~~
449 ~~showed ongoing denitrification, where Sanders et al. (2018) measured intense nitrification, anthe s. as. ,~~
450 ~~Norbistrath et al. (2022) determined intense total alkalinity generation, and Dähnke et al. (2022) found that nitrogen~~
451 ~~turnover were was driven by high particulate organic matter in this region. The highest N₂O peaks of our study~~
452 ~~were located in the Port of Hamburg. Brase et al. (2017) identified thethe HamburgHamburg port region as a~~
453 ~~hotspot of N₂O production and hypothesized that simultaneous nitrification and sediment denitrification were~~

454 responsible. We use our expanded dataset to further evaluate this hypothesis and to identify drivers for N₂O
455 production in the port region.

456

457 During all ~~our~~ cruises in spring and summer, we measured ammonium and nitrite peaks in the Hamburg Port region
458 (Fig. 2c and e, exemplary for September 2020 in Fig. ~~6b4b~~). Several researchers did address the nitrogen turnover
459 and this; accumulation of nitrite and ammonium assuming that the sudden increase of water depth in the Port leads
460 to a light limitation and decomposition of riverine organic material (Schroeder, 1997; Schöl et al., 2014). This in
461 turn raises ammonium and nitrite concentrations and fosters nitrification in the port region (Sanders et al., 2018;
462 Dähnke et al., 2022).

463 -High nitrite concentrations are favorable ~~for~~ N₂O production by nitrification and ~~of~~ nitrifier-denitrification
464 (Quick et al., 2019), ~~and while~~ low-oxygen conditions facilitate ~~made~~ both nitrification and denitrification
465 plausible in this region. We found that N₂O saturations increased with decreasing discharge (R = -0.48, Table 5)
466 during spring and summer. This further points towards in-situ N₂O production, because denitrification and
467 nitrification are more intense during longer at higher residence times (e.g. Nixon et al. 1996; Pind et al. 1997;
468 Silvennoinen et al. 2007; Gonçalves et al. 2010). Overall, our data showed the succession of ammonium, nitrite
469 and N₂O production (Fig. 4b and supplementary material S3-S13) confirming simultaneous sedimentary
470 denitrification and nitrification in the water column responsible pathways for N₂O production in the Port of
471 Hamburg (Brase et al. 2017). ~~Overall, our data show that the correlations of ammonium, nitrite and N₂O are~~
472 ~~significant and confirm that simultaneous denitrification and nitrification likely are responsible for N₂O~~
473 ~~production.~~

474 ~~A correlation analysis for the Hamburg Port region (stream kilometer 610—645) revealed a strong negative~~
475 ~~correlation of N₂O saturation with pH (R = -0.60), nitrite concentrations (R = -0.58), oxygen saturation (R = -0.58),~~
476 ~~particulate carbon (PC) content (R = -0.53) and particulate nitrogen (PN) content (R = -0.49).~~

477 In spring and summer, we found no linear relationship ~~of~~ between N₂O_{xs} and AOU in the Hamburg Port (Fig. 3).
478 This may result from combined N₂O production by nitrification and denitrification. However, oxygen saturation
479 and N₂O saturation were inversely correlated in ~~the~~ Hamburg Port (~~R = -0.58~~ Table 4 and 5), suggesting that N₂O
480 production was controlled by oxygen concentrations, and thus was related to oxygen consumption in the port
481 region. Most (75 %) of this oxygen consumption is caused by respiration whereas the remaining 25 % stem from
482 nitrification (Schöl et al., 2014; Sanders et al., 2018). This respiration in turn is determined by remineralization of
483 algal material from the upstream river that is transported to and respired within the port region (Schroeder, 1997;
484 Kerner, 2000; Schöl et al., 2014), ~~and this directly links~~ linking estuarine N₂O production to river eutrophication.
485 (Fabisik et al.; (2023) showed that algae could additionally contribute to N₂O production. In the Elbe, f
486 fresh organic matter from the Elbe r River with low C/N values as well as high PN and PC contents entered the estuary,
487 showing up in low C/N values ranging from 6.6 in July 2019 to 10.8 in August 2017, as well as in high PN and
488 high PC contents. This organic material was where it rapidly got degraded in the Hamburg Port region (Fig. S1).
489 Dähnke et al. (2022) found that labile organic matter ~~strongly~~ fueled nitrification but also denitrification in the
490 fresh water part of the Elbe E estuary, which, as shown in our study, results in high N₂O production in the Hamburg
491 Port, region leading to the reported negative correlations of PC and PN content with N₂O saturation. (~~Zander et~~
492 ~~al., 2022)~~

493 Overall ~~in spring and summer~~, oxygen conditions mainly controlled N₂O production in the Hamburg Port region
494 in spring and summer. Since respiration of organic matter dominates oxygen drawdown in the port region, we

495 deduced that N₂O production ~~there was~~ is linked to the decomposition of phytoplankton produced in the upstream
496 Elbe ~~R~~ river regions.

497 **4.4 Hamburg Port: N₂O production in winter**

498 ~~In winter, low water temperature (< 6 °C) should hamper biological production (Koch et al., 1992; Halling-~~
499 ~~Sorensen and Jorgensen, 1993). Indeed, we did not detect a N₂O peak in the MTZ in winter, but we find high N₂O~~
500 ~~concentrations in the port region. Intriguingly, we also find high N₂O concentrations in the port region in winter,~~
501 ~~at a time when low water temperature should hamper biological production. In the MTZ, the other identified region~~
502 ~~of intense estuarine N₂O production, we did not detect an N₂O peak during either March cruise. With water~~
503 ~~temperatures below 6 °C, biological processing likely was inhibited (Koch et al., 1992; Halling Sorensen and~~
504 ~~Jorgensen, 1993). For March 2022, we found a linear increase of N₂O_{xs} and AOU along with oxygen consumption~~
505 ~~and increasing ammonium, nitrite and PN concentrations indicating nitrification in the Hamburg Port port region~~
506 ~~producing N₂O. Unlike in summer, N₂O concentrations showed a flat increase extending far into the oligohaline~~
507 ~~section of the estuary (Fig. 2, ~~4d, supplementary material~~ Fig. S1).~~

508 However, in March 2021, we found a sharp and sudden increase in N₂O, with a peak concentration that by far
509 exceeded internal biological sources in summer (Fig. 2h). ~~Also, an~~ ammonium peak in the water column
510 coincided with the N₂O maximum (Fig. 2f and ~~supplementary material~~ Fig. ~~S10~~~~S11~~). If microbial activity is mostly
511 temperature-inhibited, a ~~point~~ local source of N₂O in the port seems the most likely cause. ~~(Zander et al., 2020,~~
512 ~~2022)(Deek et al., 2013) Ammonium and N₂O concentrations are high in the pore water of underlying sediments,~~
513 ~~so one potential source of elevated N₂O may be the deepening and dredging works in the Hamburg Port region,~~
514 ~~stirring up sediment. Indeed,~~

515 ~~We considered intensified deepening operations in the Port of Hamburg one potential source of elevated N₂O~~
516 ~~saturation. Deepening and dredging work occurred in the Hamburg Port region in 2021 (HPA, pers. Comm.,~~
517 ~~Karrasch 2022), ~~but~~ However, this also applied to 2022, when we saw no sharp N₂O peak (Fig. 2h). Furthermore,~~
518 ~~the regions of deepening and dredging operation did not match the region of high N₂O concentrations, and since~~
519 ~~turbidity at the time of sampling did not change significantly compared to other cruises. Jointly, this also speaks~~
520 ~~against a major signal from suggests that channel dredging and deepening was not the primary cause for the 2021~~
521 ~~winter N₂O peak. Thus, we conclude that sediment input most likely was not the source of N₂O in the water column~~
522 ~~in winter 2021.~~

523 Another possible source of N₂O is the ~~waste water treatment plant (WWTP) Köhlbrandhöft, which treats the waste~~
524 ~~water from the Hamburg metropolitan region. The WWTP outflow in the Southern Elbe that joins the sampled~~
525 ~~stretch main estuary at stream kilometer 626 (Fig. 1), matching the N₂O peak at stream kilometer 627 (Fig. 2h and~~
526 ~~3b). As explained above (section 4.3), the effect of this WWTP on N₂O saturations under normal conditions should~~
527 ~~be negligible. This peak can be the result of an extraordinary event during our sampling. We indeed found out that~~
528 ~~aggravated operation conditions in the WWTP at the time of sampling were caused by that an extreme rain event~~
529 ~~occurred on March 11th 2021 (HAMBURG WASSER, pers. Comm., Laurich 2022) with a statistical recurrence~~
530 ~~probability of one to five years (<https://sri.hamburgwasser.de/>, last access: 04.04.2023). This rare event caused~~
531 ~~aggravated operation conditions in the WWTP at the time of sampling. While the operators could still meet the~~
532 ~~limits for the effluent levels of nitrate and ammonium, higher than usual ammonium loads exited left the treatment~~
533 ~~plant during the March 2021 campaign at this time. We assume that these is elevated ammonium WWTP loads from~~
534 ~~the WWTP, were rapidly converted to N₂O as the warmer and biologically active waste water entered the Elbe~~

535 ~~Estuary most likely was the cause of the unexpected high N₂O peak in March 2021.~~ An important factor for
536 ~~aggravated conditions was a temperature drop in the WWTP caused by cold rain water, we hypothesize that a~~
537 ~~similar rain event in warmer months would not lead to comparable N₂O peaks.~~ ▯

538 Therefore, we argue that our March 2021 cruise likely represents an exception due to an extreme weather situation,
539 ~~and that typical~~ whereas normal winter conditions in the ~~Elbe~~ estuary comply with the N₂O production, ~~as-like~~ in
540 March 2022.

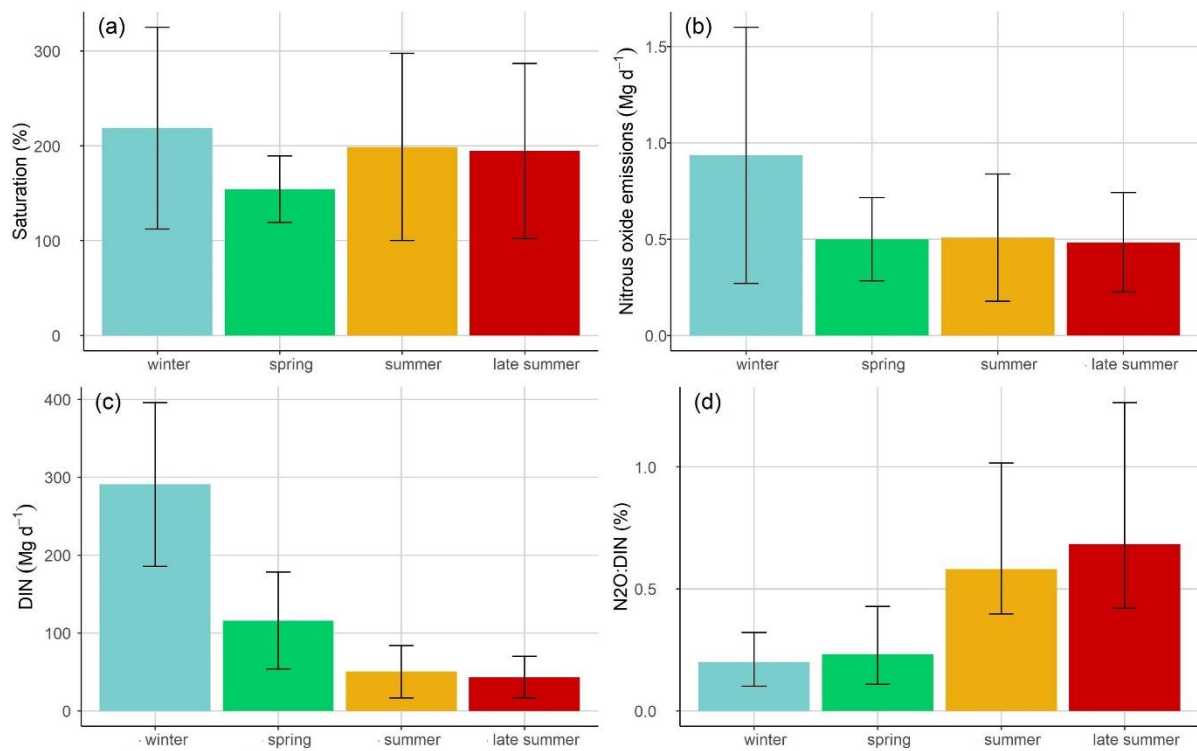
541 **4.5 Seasonally varying changes of N₂O emissions-N₂O:DIN dynamic**

542 We calculated annual N₂O emissions of the Elbe Estuary ranging from 0.08 ± 0.03 Gg-N₂O yr⁻¹ to
543 0.25 ± 0.16 Gg-N₂O yr⁻¹, which varied from recent N₂O summer emission estimate of 0.18 ± 0.01 Gg-N₂O yr⁻¹ by
544 Brase et al. (2017). Estuarine N₂O emissions are affected by tides, diel variations and currents (Barnes et al., 2006;
545 Baulch et al., 2012; Gonçalves et al., 2015), all of which we did not address in our study. Range of possible
546 parametrizations of gas transfer coefficients further complicates a direct comparison of fluxes between studies
547 (Hall Jr. and Ulseth, 2020; Rosentreter et al., 2021), which were reflected in the big differences of our emission
548 estimates (Table 2). Therefore, a direct comparison to other studies is difficult.

549 In a more general approach, the relationship between N₂O and DIN (N₂O:DIN) is used for global estimates of N₂O
550 emissions (Kroeze et al., 2005, 2010; Ivens et al., 2011; Hu et al., 2016). Using publicly available data (Table S4
551 and S5), we calculated the amount of the annual nitrogen load released as N₂O. Depending on the parametrization
552 used for the gas transfer coefficients, 0.14 % to 0.67 % of the annual DIN loads of the Elbe Estuary were released
553 as N₂O (0.11 % to 0.57 % for TN loads). This is significantly less than the 1 % predicted by Kroeze et al. (2005),
554 but matches results from other estuaries with high agricultural input, e.g. Wells et al. (2018) with 0.3 % to 0.7 %
555 (0.1 % for TN loads) and Robinson et al. (1998) with 0.5 % (0.3 % for TN loads) as well as the 0.11 % to 0.37 %
556 estimated by (Maavara et al., 2019), who used TN loads to predict global estuarine emissions.

557 At our site, highest emissions were estimated in winter (Fig. 5b) along with highest DIN loads (Fig. 5c). In spring,
558 summer and late summer, N₂O emissions reduced along with DIN loads (Fig. 5b, c). However, N₂O release did
559 not scale with the seasonal change of DIN. In winter, 0.10 % to 0.32 % of DIN were released as N₂O, whereas
560 during the other seasons, up to 1.26 % were emitted. Thus, our results corroborate that there is a deviating
561 relationship between DIN and N₂O (Borges et al., 2015; Marzadri et al., 2017; Wells et al., 2018) showing that
562 this relationship even varies seasonally on site due to changing drivers for N₂O production and emissions.

563 Next to DIN loads, we find that organic matter is an important driver for N₂O production by providing substrate
564 for nitrification. Furthermore, the comparison of our results with previous measurements in the Elbe Estuary
565 revealed that N₂O saturation stopped to scale with DIN input after the 1990s (section 4.1). The significant regime
566 change after the 1990s enabled phytoplankton growth to reestablish in the river (Kerner, 2000; Amann et al., 2012;
567 Hillebrand et al., 2018; Rewrie et al., submitted) and led to high nitrification rates in the estuary (Dähnke et al.,
568 2008; Sanders et al., 2018), supporting the overarching control of organic matter on N₂O production and emissions
569 along the Elbe Estuary.



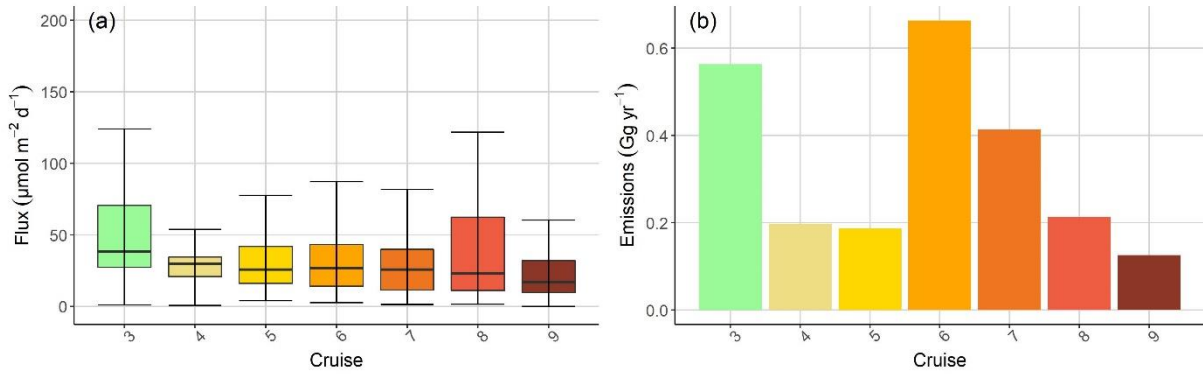
570

571 **Figure 5: (a) Average nitrous oxide saturation for each season, (b) average nitrous oxide emissions for each season**
 572 **calculated after Borges et al. (2004), (c) average DIN loads for each season and (d) ratio of nitrous oxide emissions and**
 573 **DIN loads (N₂O:DIN) for each season. The error bars represent the standard deviations for (a), (b) and (c). The**
 574 **N₂O:DIN ratios is shown as average values calculated for each parametrization and wind speeds with error bars**
 575 **representing their variability.**

576 (Kerner, 2000; Amann et al., 2012; Hillebrand et al., 2018; Rewrie et al., submitted)

577 For an accurate assessment of annual estuarine N₂O emissions, we first evaluate their seasonal distribution. In
 578 March, average N₂O emissions were 0.28 ± 0.17 Gg yr⁻¹. Note that we deliberately excluded the N₂O peak in
 579 March 2021 and interpolated the concentrations in this region to exclude the effect of a point source (Section 4.4).
 580 Nonetheless, high wind speeds still led to high N₂O emissions in March 2021 (Tab. 3). March 2022 (0.16 ± 0.08
 581 Gg yr⁻¹) only slightly deviated from average N₂O emissions in spring and summer (0.20 ± 0.05 Gg yr⁻¹). Overall,
 582 we calculated average annual emissions using the seasonal averages (Tab. 3) resulting in 0.24 ± 0.06 Gg yr⁻¹, thus
 583 exceeding the recent summer N₂O emission estimates of 0.18 ± 0.01 Gg yr⁻¹ by Brase et al. (2017).

584 Enhanced microbial N₂O production can lead to high N₂O flux densities in summer (Usui et al., 2001; Allen et al.,
 585 2011; Murray et al., 2015; Quick et al., 2019), as is the case for the Elbe estuary in spring and summer (Fig. 7).
 586 However, winter flux densities were unexpectedly high (Fig. 7). Elevated winter N₂O emissions originated from
 587 1) high wind speeds with increased sea-air exchange, 2) nitrification in the Hamburg Port and 3) elevated riverine
 588 N₂O inputs into the estuary, with 25 nmol L^{-1} (161.9% saturation) and 26 nmol L^{-1} (165.3% saturation) in March
 589 2021 and 2022, respectively, well above summer riverine input concentrations. Since the Elbe estuary acted as a
 590 transport channel, rather than a bioreactor in the winter months, due to temperature inhibited biological processing
 591 (Koch et al., 1992; Halling-Sorensen and Jorgensen, 1993), the N₂O concentrations remained high until mixing
 592 with water from the North Sea, which resulted in a decrease and in outgassing to the atmosphere.



593 **Figure 7: (a) Monthly variation of N₂O flux density in µmol m⁻² d⁻¹, (b) monthly variation of N₂O emissions in Gg yr⁻¹.**

595 The high riverine N₂O input into the estuary is intriguing and may be caused by high nitrate discharge from soils and groundwater fueling N₂O production, which was found in other streams and rivers (Beaulieu et al., 2009; Clough et al., 2011). Agricultural fertilizer application might also affect winter N₂O concentrations (Murray et al., 2015), since it can lead to high DIN and N₂O concentrations in estuaries. In the 1990s, Hanke and Knauth (1990) also measured high riverine N₂O concentrations in the Elbe estuary in winter, albeit at higher DIN concentrations. Other temperate estuaries showed high N₂O emissions with the dominant control on N₂O concentrations being freshwater delivery, rather than in-situ production (Barnes and Owens, 1999; Robinson et al., 1998; Murray et al., 2020). In combination with a higher probability of strong winds in winter, it is clear that winter N₂O emissions in the Elbe estuary should not be neglected, as they can potentially even exceed summer emissions.

604 Overall in winter, large nitrogen loads from the Elbe catchment caused high riverine N₂O concentrations, which led to high N₂O emissions in the adjacent estuary (Fig. 7). In summer, reduced riverine N₂O input was compensated by in-situ N₂O production processes. We find that both effects are currently balanced, leading to year-round high N₂O emissions in this estuary.

608 **Table 3: Average N₂O flux densities and emissions for spring and summer, winter and per year. For the winter, only the March 2022 cruise was used due to the extreme peak in 2021 that was most probably caused by a point-source influx of ammonium and an extreme weather event. For the emissions calculation, the area of the Elbe estuary of 371.85 km² was taken into account (Brase et al., 2017).**

Season	Average N ₂ O flux densities	N ₂ O emissions
Spring and summer	33.5 ± 7.8 µmol m ⁻² d ⁻¹	0.20 ± 0.05 Gg yr ⁻¹
March	47.3 ± 28.1 µmol m ⁻² d ⁻¹	0.28 ± 0.17 Gg yr ⁻¹
Annual average	40.3 ± 14.3 µmol m ⁻² d ⁻¹	0.24 ± 0.06 Gg yr ⁻¹

612 5 Conclusions

613 Overall, the Elbe is a year-round source of N₂O to the atmosphere, with highest emission occurring in winter, along with high DIN loads and high wind speeds. However, summer N₂O saturation and emissions did not decrease with lower riverine nitrogen input suggesting variable relations of DIN and N₂O (Borges et al., 2004; Marzadri et al., 2017; Wells et al., 2018), and seasonal variability of this ratio caused by changing drivers for N₂O production and emissions. Two hot-spots of N₂O production were found in the Elbe estuary: the Port of Hamburg and the mesohaline estuary near the estuarine turbidity maximum. Biological N₂O production was enhanced by warmer temperatures and fueled by riverine organic matter in the Hamburg Port or marine organic matter in the MTZ. A comparison with historical N₂O measurements in the Elbe Estuary revealed that N₂O saturation sealedid

621 ~~not decrease with DIN input after the 1990s. The improvement of water quality in the Elbe Estuary allowed~~
622 ~~phytoplankton growth after the reunification of Germany in 1990s (Kerner, 2000; Amann et al., 2012; Hillebrand~~
623 ~~et al., 2018; Rewrie et al., submitted) and led to a switch from dominant denitrification to high nitrification (Dähnke~~
624 ~~et al., 2008; Sanders et al., 2018), supporting the overarching control of organic matter on N₂O production along~~
625 ~~the Elbe Estuary (Dähnke et al., 2008; Sanders et al., 2018). Thus, our findings indicate that DIN availability is not~~
626 ~~the sole control of N₂O production in N₂O emissions in estuaries with high agricultural input. High organic matter~~
627 ~~availability due to phytoplankton blooms driven by river eutrophication fuels nitrification and subsequent and this~~
628 ~~are also essential, N₂O emissions, causing a decoupling of the N₂O:DIN ratio. Therefore, N₂O emissions in heavily~~
629 ~~managed estuaries with high agricultural loads are clearly linked to eutrophication. was~~
630 ~~Consequently, reducing nitrogen input alone is not sufficient to minimize N₂O emissions from estuaries. Further~~
631 ~~measures are needed to prevent the developments of intense phytoplankton blooms in rivers and estuaries.~~
632 ~~Especially considering climate change projections of more frequent and extensive draughts and warmer~~
633 ~~temperatures (IPCC, 2022), which potentially fuel phytoplankton growth (e.g. Scharfe et al., 2009; Kamjunke et~~
634 ~~al., 2021; IPCC, 2022). Overall, we found enhanced N₂O concentrations along the entire Elbe estuary, which point~~
635 ~~towards in-situ N₂O production that compensated the effect of decreasing DIN loads since the 1990s. Two hot~~
636 ~~spots of N₂O production were found in the estuary: the Port of Hamburg and the mesohaline estuary near the~~
637 ~~estuarine turbidity maximum. Biological N₂O production was enhanced by warmer temperatures and fueled by~~
638 ~~riverine organic matter in the Hamburg Port or marine organic matter in the MTZ.~~
639 ~~We saw no seasonality in N₂O emissions, despite seasonal variations in in-situ N₂O production: In winter, high~~
640 ~~riverine N₂O input led to high N₂O saturation and emissions in the estuary, whereas in summer, high N₂O emissions~~
641 ~~were controlled by in-situ production. Overall, the Elbe estuary is a year-round perennial source of N₂O, with~~
642 ~~estimated annual emissions of 0.24 ± 0.06 Gg yr⁻¹. In conjunction with the overarching control of N₂O production~~
643 ~~by organic matter quality, this highlights that a holistic approach of water quality improvement and nutrient~~
644 ~~mitigation is needed to further reduce N₂O emission from the Elbe estuary.~~

645 **Data availability**

646 The dataset generated and/or analyzed in this study are currently available upon request from the corresponding
647 author and will be made publicly available under coastMap Geoportal (www.coastmap.org) connecting to
648 PANGAEA. (<https://www.pangaea.de/>) with DOI availability in the near future.

649 **Authors contribution**

650 GS, TS and KD designed this study. GS did the sampling and measurements for cruises from 2020 to 2022 as well
651 as the data interpretation and evaluation. TS was responsible for the sampling and measurements for cruises done
652 in 2017 and 2019. YGV provided the oxygen data correction from the FerryBox data. KD, HWB, YGV and TS
653 contributed with scientific and editorial recommendations. GS prepared the manuscript with contributions of all
654 co-authors.

655 **Competing interest**

656 The authors declare that they have no conflict of interest.

657 **Acknowledgments**

658 This study was funded by the Deutsche Forschungsgemeinschaft (DFG, German Research Foundation) under
659 Germany's Excellence Strategy – EXC 2037 “CLICCS - Climate, Climatic Change, and Society” – Project
660 Number: 390683824, contribution to the Center for Earth System Research and Sustainability (CEN) of Universität
661 Hamburg. Parts of the study were done in the framework of the cross-topic activity MOSES (Modular Observation
662 Solutions for Earth Systems) within the Helmholtz program Changing Earth (Topic 4.1). We thank the crew of
663 R/V Ludwig Prandtl for the great support during the cruises. Thanks to Leon Schmidt and the entire working group
664 “Aquatic nutrients cycles” for measuring nutrients and the support during the campaigns. We are thankful for the
665 Hereon FerryBox Team for providing the FerryBox data. Thanks to the working group of Biogeochemistry at the
666 Institute for Geology of the University Hamburg for measuring C/N ratios, PC and PN fractions. We thank Frank
667 Laurich (HAMBURG WASSER) and Dr. Maja Karrasch (Hamburg Port Authority) for their interest in our N₂O
668 measurements and their willingness to provide information. [Thanks to Victoria Ortiz \(Federal Waterways and
669 Engineering and Research Institute\) for providing the respective areas of the Elbe Estuary.](#) Thanks to the NOAA
670 ESRL GML CCGG Group for providing high quality, readily accessible atmospheric N₂O data.

671 **References**

- 672 Amann, T., Weiss, A., and Hartmann, J.: Carbon dynamics in the freshwater part of the Elbe estuary, Germany:
673 Implications of improving water quality, *Estuar. Coast. Shelf Sci.*, 107, 112–121,
674 <https://doi.org/10.1016/j.ecss.2012.05.012>, 2012.
- 675 Bange, H. W.: Nitrous oxide and methane in European coastal waters, *Estuar. Coast. Shelf Sci.*, 70, 361–374,
676 <https://doi.org/10.1016/j.ecss.2006.05.042>, 2006.
- 677 Bange, H. W.: Chapter 2 - Gaseous Nitrogen Compounds (NO, N₂O, N₂, NH₃) in the Ocean, *Nitrogen Mar.
678 Environ. Second Ed.*, 51–94, <https://doi.org/10.1016/B978-0-12-372522-6.00002-5>, 2008.
- 679 Barnes, J. and Owens, N. J. P.: Denitrification and Nitrous Oxide Concentrations in the Humber Estuary, UK, and
680 Adjacent Coastal Zones, *Mar. Pollut. Bull.*, 37, 247–260, [https://doi.org/10.1016/S0025-326X\(99\)00079-X](https://doi.org/10.1016/S0025-326X(99)00079-X), 1999.
- 681 Barnes, J. and Upstill-Goddard, R. C.: N₂O seasonal distributions and air-sea exchange in UK estuaries:
682 Implications for the tropospheric N₂O source from European coastal waters, *J. Geophys. Res. Biogeosciences*,
683 116, <https://doi.org/10.1029/2009JG001156>, 2011.
- 684 Barnes, J., Ramesh, R., Purvaja, R., Nirmal Rajkumar, A., Senthil Kumar, B., Krithika, K., Ravichandran, K.,
685 Uher, G., and Upstill-Goddard, R.: Tidal dynamics and rainfall control N₂O and CH₄ emissions from a pristine
686 mangrove creek, *Geophys. Res. Lett.*, 33, <https://doi.org/10.1029/2006GL026829>, 2006.
- 687 Baulch, H. M., Dillon, P. J., Maranger, R., Venkiteswaran, J. J., Wilson, H. F., and Schiff, S. L.: Night and day:
688 short-term variation in nitrogen chemistry and nitrous oxide emissions from streams, *Freshw. Biol.*, 57, 509–525,
689 <https://doi.org/10.1111/j.1365-2427.2011.02720.x>, 2012.
- 690 BAW, Ortiz, V.: pers. Comm.: Flächen des Elbe Ästuars, 2023.
- 691 Beaulieu, J. J., Shuster, W. D., and Rebholz, J. A.: Nitrous Oxide Emissions from a Large, Impounded River: The
692 Ohio River, *Environ. Sci. Technol.*, 44, 7527–7533, <https://doi.org/10.1021/es1016735>, 2010.
- 693 Bergemann, M.: Die Trübungszone in der Tideelbe - Beschreibung der räumlichen und zeitlichen Entwicklung,
694 Wassergütestelle Elbe, 2004.
- 695 Bergemann, M. and Gaumert, T.: Elbebericht 2008: Ergebnisse des nationalen Überwachungsprogramms Elbe der
696 Bundesländer über den ökologischen und chemischen Zustand der Elbe nach EG-WRRL sowie der

- 697 Trendentwicklung von Stoffen und Schadstoffgruppen, Flussgebietsgemeinschaft Elbe (FGG Elbe), Hamburg,
698 2008.
- 699 van Beusekom, J. E. E., Carstensen, J., Dolch, T., Grage, A., Hofmeister, R., Lenhart, H., Kerimoglu, O., Kolbe,
700 K., Pätsch, J., Rick, J., Rönn, L., and Rüter, H.: Wadden Sea Eutrophication: Long-Term Trends and Regional
701 Differences, *Front. Mar. Sci.*, 6, 370, <https://doi.org/10.3389/fmars.2019.00370>, 2019.
- 702 Bianchi, T. S.: *Biogeochemistry of Estuaries*, Oxford University Press, New York, 706 pp., 2007.
- 703 Boehlich, M. J. and Strotmann, T.: The Elbe Estuary, *Küste*, 74, 288–306, 2008.
- 704 Boehlich, M. J. and Strotmann, T.: Das Elbeästuar, *Küste*, 87, Kuratorium für Forschung im Küsteningenieurwesen
705 (KFKI), <https://doi.org/10.18171/1.087106>, 2019.
- 706 Borges, A., Vanderborght, J.-P., Schiettecatte, L.-S., Gazeau, F., Ferrón-Smith, S., Delille, B., and Frankignoulle,
707 M.: Variability of gas transfer velocity of CO₂ in a macrotidal estuary (The Scheldt), *Estuaries*, 27, 593–603,
708 <https://doi.org/10.1007/BF02907647>, 2004.
- 709 Borges, A. V., Darchambeau, F., Teodoru, C. R., Marwick, T. R., Tamooh, F., Geeraert, N., Omengo, F. O.,
710 Guérin, F., Lambert, T., Morana, C., Okuku, E., and Bouillon, S.: Globally significant greenhouse-gas emissions
711 from African inland waters, *Nat. Geosci.*, 8, 637–642, <https://doi.org/10.1038/ngeo2486>, 2015.
- 712 Bouwman, A. F., Bierkens, M. F. P., Griffioen, J., Hefting, M. M., Middelburg, J. J., Middelkoop, H., and Slomp,
713 C. P.: Nutrient dynamics, transfer and retention along the aquatic continuum from land to ocean: towards
714 integration of ecological and biogeochemical models, *Biogeosciences*, 10, 1–23, [https://doi.org/10.5194/bg-10-1-](https://doi.org/10.5194/bg-10-1-2013)
715 2013, 2013.
- 716 Brase, L., Bange, H. W., Lendt, R., Sanders, T., and Dähnke, K.: High Resolution Measurements of Nitrous Oxide
717 (N₂O) in the Elbe Estuary, *Front. Mar. Sci.*, 4, 162, <https://doi.org/10.3389/fmars.2017.00162>, 2017.
- 718 Büttner, O., Jawitz, J. W., and Borchardt, D.: Ecological status of river networks: stream order-dependent impacts
719 of agricultural and urban pressures across ecoregions, *Environ. Res. Lett.*, 15, 1040b3,
720 <https://doi.org/10.1088/1748-9326/abb62e>, 2020.
- 721 Clark, J. F., Schlosser, P., Simpson, H. J., Stute, M., Wanninkhof, R., and Ho, D. T.: Relationship between gas
722 transfer velocities and wind speeds in the tidal Hudson River determined by the dual tracer technique, in: *Air-*
723 *Water Gas Transfer*, edited by: Jähne, B. and Monahan, E. C., AEON Verlag, Hanau, 785–800, 1995.
- 724 Crossland, C. J., Baird, D., Ducrotoy, J.-P., Lindeboom, H., Buddemeier, R. W., Dennison, W. C., Maxwell, B.
725 A., Smith, S. V., and Swaney, D. P.: The Coastal Zone — a Domain of Global Interactions, in: *Coastal Fluxes in*
726 *the Anthropocene: The Land-Ocean Interactions in the Coastal Zone Project of the International Geosphere-*
727 *Biosphere Programme*, edited by: Crossland, C. J., Kremer, H. H., Lindeboom, H. J., Marshall Crossland, J. I., and
728 Le Tissier, M. D. A., Springer, Berlin, Heidelberg, 1–37, https://doi.org/10.1007/3-540-27851-6_1, 2005.
- 729 Dähnke, K., Bahlmann, E., and Emeis, K.-C.: A nitrate sink in estuaries? An assessment by means of stable nitrate
730 isotopes in the Elbe estuary, *Limnol. Oceanogr.*, 53, 1504–1511, <https://doi.org/10.4319/lo.2008.53.4.1504>, 2008.
- 731 Dähnke, K., Sanders, T., Voynova, Y., and Wankel, S. D.: Nitrogen isotopes reveal a particulate-matter-driven
732 biogeochemical reactor in a temperate estuary, *Biogeosciences*, 19, 5879–5891, [https://doi.org/10.5194/bg-19-](https://doi.org/10.5194/bg-19-5879-2022)
733 5879-2022, 2022.
- 734 Deek, A., Dähnke, K., van Beusekom, J., Meyer, S., Voss, M., and Emeis, K.-C.: N₂ fluxes in sediments of the
735 Elbe Estuary and adjacent coastal zones, *Mar. Ecol. Prog. Ser.*, 493, 9–21, <https://doi.org/10.3354/meps10514>,
736 2013.
- 737 Dlugokencky, E. J., Crotwell, A. M., Mund, J. W., Crotwell, M. J., and Thoning, K. W.: Earth System Research
738 Laboratory Carbon Cycle and Greenhouse Gases Group Flask-Air Sample Measurements of N₂O at Global and
739 Regional Background Sites, 1967-Present [Data set], <https://doi.org/10.15138/53G1-X417>, 2022.

- 740 Fabisik, F., Guieysse, B., Procter, J., and Plouviez, M.: Nitrous oxide (N₂O) synthesis by the freshwater
741 cyanobacterium *Microcystis aeruginosa*, *Biogeosciences*, 20, 687–693, <https://doi.org/10.5194/bg-20-687-2023>,
742 2023.
- 743 FGG Elbe: Nährstoffminderungsstrategie für die Flussgebietsgemeinschaft Elbe, Flussgebietsgemeinschaft Elbe
744 (FGG Elbe), Magdeburg, 2018.
- 745 Das Fachinformationssystem (FIS) der FGG Elbe: [https://www.elbe-
datenportal.de/FisFggElbe/content/start/ZurStartseite.action;jsessionid=A37EDCF5B5EC1ECB15091447E64EC
538](https://www.elbe-
746 datenportal.de/FisFggElbe/content/start/ZurStartseite.action;jsessionid=A37EDCF5B5EC1ECB15091447E64EC
747 538), last access: 21 November 2022.
- 748 Fraga, F., Ríos, A. F., Pérez, F. F., and Figueiras, F. G.: Theoretical limits of oxygen:carbon and oxygen:nitrogen
749 ratios during photosynthesis and mineralisation of organic matter in the sea, *Sci. Mar.*, 62, 161–168,
750 <https://doi.org/10.3989/scimar.1998.62n1-2161>, 1998.
- 751 Garnier, J., Cébron, A., Talleg, G., Billen, G., Sebilo, M., and Martinez, A.: Nitrogen Behaviour and Nitrous Oxide
752 Emission in the Tidal Seine River Estuary (France) as Influenced by Human Activities in the Upstream Watershed,
753 *Biogeochemistry*, 77, 305–326, <https://doi.org/10.1007/s10533-005-0544-4>, 2006.
- 754 Gaumert, T. and Bergemann, M.: Sauerstoffgehalt der Tideelbe - Entwicklung der kritischen Sauerstoffgehalte im
755 Jahr 2007 und in den Vorjahren, Erörterung möglicher Ursachen und Handlungsoptionen,
756 Flussgebietsgemeinschaft Elbe, 2007.
- 757 Geerts, L., Wolfstein, K., Jacobs, S., van Damme, S., and Vandenbruwaene, W.: Zonation of the TIDE estuaries,
758 TIDE toolbox, 2012.
- 759 Gonçalves, C., Brogueira, M. J., and Camões, M. F.: Seasonal and tidal influence on the variability of nitrous oxide
760 in the Tagus estuary, Portugal, *Sci. Mar.*, 74, 57–66, <https://doi.org/10.3989/scimar.2010.74s1057>, 2010.
- 761 Gonçalves, C., Brogueira, M. J., and Nogueira, M.: Tidal and spatial variability of nitrous oxide (N₂O) in Sado
762 estuary (Portugal), *Estuar. Coast. Shelf Sci.*, 167, 466–474, <https://doi.org/10.1016/j.ecss.2015.10.028>, 2015.
- 763 Hall Jr., R. O. and Ulseth, A. J.: Gas exchange in streams and rivers, *WIREs Water*, 7, e1391,
764 <https://doi.org/10.1002/wat2.1391>, 2020.
- 765 Halling-Sorensen, B. and Jorgensen, S. E. (Eds.): 3. Process Chemistry and Biochemistry of Nitrification, in:
766 *Studies in Environmental Science*, vol. 54, Elsevier, 55–118, [https://doi.org/10.1016/S0166-1116\(08\)70525-9](https://doi.org/10.1016/S0166-1116(08)70525-9),
767 1993.
- 768 HAMBURG WASSER, Laurich, F.: pers. Comm.: N₂O in der Elbe, 2022.
- 769 Hanke, V.-R. and Knauth, H.-D.: N₂O-Gehalte in Wasser-und Luftproben aus den Bereichen der Tideelbe und der
770 Deutschen Bucht, GKSS-Forschungszentrum, Weinheim, 1990.
- 771 Hansen, H. P. and Koroleff, F.: Determination of nutrients, in: *Methods of Seawater Analysis*, John Wiley & Sons,
772 Ltd, 159–228, <https://doi.org/10.1002/9783527613984.ch10>, 1999.
- 773 Harley, J. F., Carvalho, L., Dudley, B., Heal, K. V., Rees, R. M., and Skiba, U.: Spatial and seasonal fluxes of the
774 greenhouse gases N₂O, CO₂ and CH₄ in a UK macrotidal estuary, *Estuar. Coast. Shelf Sci.*, 153, 62–73,
775 <https://doi.org/10.1016/j.ecss.2014.12.004>, 2015.
- 776 Hedges, J. I. and Keil, R. G.: Sedimentary organic matter preservation: an assessment and speculative synthesis,
777 *Mar. Chem.*, 49, 81–115, [https://doi.org/10.1016/0304-4203\(95\)00008-F](https://doi.org/10.1016/0304-4203(95)00008-F), 1995.
- 778 Hein, S. S. V., Sohr, V., Nehlsen, E., Strotmann, T., and Fröhle, P.: Tidal Oscillation and Resonance in Semi-
779 Closed Estuaries—Empirical Analyses from the Elbe Estuary, North Sea, *Water*, 13, 848,
780 <https://doi.org/10.3390/w13060848>, 2021.
- 781 Schleswig-Holstein u. Hamburg: Mittlere Windgeschwindigkeit (1986-2015)* | Norddeutscher Klimamonitor:
782 [https://www.norddeutscher-klimamonitor.de/klima/1986-2015/jahr/mittlere-windgeschwindigkeit/schleswig-
holstein-hamburg/coastdat-1.html](https://www.norddeutscher-klimamonitor.de/klima/1986-2015/jahr/mittlere-windgeschwindigkeit/schleswig-
783 holstein-hamburg/coastdat-1.html), last access: 27 April 2023.

784 Hillebrand, G., Hardenbicker, P., Fischer, H., Otto, W., and Vollmer, S.: Dynamics of total suspended matter and
785 phytoplankton loads in the river Elbe, *J. Soils Sediments*, 18, 3104–3113, [https://doi.org/10.1007/s11368-018-](https://doi.org/10.1007/s11368-018-1943-1)
786 1943-1, 2018.

787 Hofmann, J., Behrendt, H., Gilbert, A., Janssen, R., Kannen, A., Kappenberg, J., Lenhart, H., Lise, W., Nunneri,
788 C., and Windhorst, W.: Catchment–coastal zone interaction based upon scenario and model analysis: Elbe and the
789 German Bight case study, *Reg. Environ. Change*, 5, 54–81, <https://doi.org/10.1007/s10113-004-0082-y>, 2005.

790 HPA and Freie und Hansestadt Hamburg: Deutsches Gewässerkundliches Jahrbuch - Elbegebiet, Teil III, Untere
791 Elbe ab der Havelmündung - 2014, Hamburg, 2017.

792 HPA, Karrasch, M.: pers. Comm.: Anfrage wegen N2OPeak - Baggerarbeiten Elbe März 2021 und März 2022,
793 2022.

794 Hu, M., Chen, D., and Dahlgren, R. A.: Modeling nitrous oxide emission from rivers: a global assessment, *Glob.*
795 *Change Biol.*, 22, 3566–3582, <https://doi.org/10.1111/gcb.13351>, 2016.

796 IKSE: Strategie zur Minderung der Nährstoffeinträge in Gewässer in der internationalen Flussgebietsgemeinschaft
797 Elbe, Internationale Kommission zur Schutz der Elbe, Magdeburg, 2018.

798 IPCC: Climate Change 2021: The Physical Science Basis. Contribution of Working Group I to the Sixth
799 Assessment Report of the Intergovernmental Panel on Climate Change, edited by: Masson-Delmotte, V., Zhai, P.,
800 Pirani, A., Connors, S. L., Péan, C., Berger, S., Caud, N., Chen, Y., Goldfarb, L., Gomis, M. I., Huang, M., Leitzell,
801 K., Lonnoy, E., Matthews, J. B. R., Maycock, T. K., Waterfield, T., Yelekçi, Ö., Yu, R., and Zhou, B., Cambridge
802 University Press, Cambridge, United Kingdom and New York, NY, USA,
803 <https://doi.org/10.1017/9781009157896>, 2021.

804 IPCC: Climate Change 2022: Impacts, Adaptation and Vulnerability. Contribution of Working Group II to the
805 Sixth Assessment Report of the Intergovernmental Panel on Climate Change., edited by: Pörtner, H.-O., Roberts,
806 D. C., Tignor, M. M. B., Poloczanska, E. S., Mintenbeck, K., Alegría, A., Craig, M., Langsdorf, S., Löschke, S.,
807 Möller, V., Okem, A., and Rama, B., Cambridge University Press, Cambridge, UK and New York, NY, USA,
808 3056 pp., <https://doi.org/10.1017/9781009325844>, 2022.

809 Ivens, W. P. M. F., Tysmans, D. J. J., Kroeze, C., Löhr, A. J., and van Wijnen, J.: Modeling global N2O emissions
810 from aquatic systems, *Curr. Opin. Environ. Sustain.*, 3, 350–358, <https://doi.org/10.1016/j.cosust.2011.07.007>,
811 2011.

812 Ji, Q., Frey, C., Sun, X., Jackson, M., Lee, Y.-S., Jayakumar, A., Cornwell, J. C., and Ward, B. B.: Nitrogen and
813 oxygen availabilities control water column nitrous oxide production during seasonal anoxia in the Chesapeake
814 Bay, *Biogeosciences*, 15, 6127–6138, <https://doi.org/10.5194/bg-15-6127-2018>, 2018.

815 Johannsen, A., Dähnke, K., and Emeis, K.: Isotopic composition of nitrate in five German rivers discharging into
816 the North Sea, *Org. Geochem.*, 39, 1678–1689, <https://doi.org/10.1016/j.orggeochem.2008.03.004>, 2008.

817 Kamjunke, N., Rode, M., Baborowski, M., Kunz, J., Zehner, J., Borchardt, D., and Weitere, M.: High irradiation
818 and low discharge promote the dominant role of phytoplankton in riverine nutrient dynamics, *Limnol. Oceanogr.*,
819 66, <https://doi.org/10.1002/lno.11778>, 2021.

820 Kappenberg, J. and Fanger, H.-U.: Sedimenttransportgeschehen in der tidebeeinflussten Elbe, der Deutschen Bucht
821 und in der Nordsee, GKSS-Forschungszentrum, Geesthacht, 2007.

822 Kassambara, A.: ggpubr: “ggplot2” Based Publication Ready Plots, 2023.

823 Kerner, M.: Interactions between local oxygen deficiencies and heterotrophic microbial processes in the elbe
824 estuary, *Limnologica*, 30, 137–143, [https://doi.org/10.1016/S0075-9511\(00\)80008-0](https://doi.org/10.1016/S0075-9511(00)80008-0), 2000.

825 Knowles, R.: Denitrification, *Microbiol. Rev.*, 46, 43–70, <https://doi.org/10.1128/mr.46.1.43-70.1982>, 1982.

826 Koch, M. S., Maltby, E., Oliver, G. A., and Bakker, S. A.: Factors controlling denitrification rates of tidal mudflats
827 and fringing salt marshes in south-west England, *Estuar. Coast. Shelf Sci.*, 34, 471–485,
828 [https://doi.org/10.1016/S0272-7714\(05\)80118-0](https://doi.org/10.1016/S0272-7714(05)80118-0), 1992.

- 829 Kroeze, C., Dumont, E., and Seitzinger, S. P.: New estimates of global emissions of N₂O from rivers and estuaries,
830 *Environ. Sci.*, 2, 159–165, <https://doi.org/10.1080/15693430500384671>, 2005.
- 831 Kroeze, C., Dumont, E., and Seitzinger, S.: Future trends in emissions of N₂O from rivers and estuaries, *J. Integr.*
832 *Environ. Sci.*, 7, 71–78, <https://doi.org/10.1080/1943815X.2010.496789>, 2010.
- 833 Maavara, T., Lauerwald, R., Laruelle, G. G., Akbarzadeh, Z., Bouskill, N. J., Van Cappellen, P., and Regnier, P.:
834 Nitrous oxide emissions from inland waters: Are IPCC estimates too high?, *Glob. Change Biol.*, 25, 473–488,
835 <https://doi.org/10.1111/gcb.14504>, 2019.
- 836 Marzadri, A., Dee, M. M., Tonina, D., Bellin, A., and Tank, J. L.: Role of surface and subsurface processes in
837 scaling N₂O emissions along riverine networks, *Proc. Natl. Acad. Sci.*, 114, 4330–4335,
838 <https://doi.org/10.1073/pnas.1617454114>, 2017.
- 839 Middelburg, J. J. and Herman, P. M. J.: Organic matter processing in tidal estuaries, *Mar. Chem.*, 106, 127–147,
840 <https://doi.org/10.1016/j.marchem.2006.02.007>, 2007.
- 841 Middelburg, J. J. and Nieuwenhuize, J.: Uptake of dissolved inorganic nitrogen in turbid, tidal estuaries, *Mar.*
842 *Ecol.-Prog. Ser.*, 192, 79–88, <https://doi.org/10.3354/meps192079>, 2000.
- 843 Murray, R. H., Erler, D. V., and Eyre, B. D.: Nitrous oxide fluxes in estuarine environments: response to global
844 change, *Glob. Change Biol.*, 21, 3219–3245, <https://doi.org/10.1111/gcb.12923>, 2015.
- 845 Nevison, C., Butler, J. H., and Elkins, J. W.: Global distribution of N₂O and the Δ N₂O-AOU yield in the
846 subsurface ocean, *Glob. Biogeochem. Cycles*, 17, 1119, <https://doi.org/10.1029/2003GB002068>, 2003.
- 847 Nightingale, P. D., Malin, G., Law, C. S., Watson, A. J., Liss, P. S., Liddicoat, M. I., Boutin, J., and Upstill-
848 Goddard, R. C.: In situ evaluation of air-sea gas exchange parameterizations using novel conservative and volatile
849 tracers, *Glob. Biogeochem. Cycles*, 14, 373–387, <https://doi.org/10.1029/1999GB900091>, 2000.
- 850 Nixon, S. W., Ammerman, J. W., Atkinson, L. P., Berounsky, V. M., Billen, G., Boicourt, W. C., Boynton, W. R.,
851 Church, T. M., Ditoro, D. M., Elmgren, R., Garber, J. H., Giblin, A. E., Jahnke, R. A., Owens, N. J. P., Pilson, M.
852 E. Q., and Seitzinger, S. P.: The fate of nitrogen and phosphorus at the land-sea margin of the North Atlantic
853 Ocean, *Biogeochemistry*, 35, 141–180, <https://doi.org/10.1007/BF02179826>, 1996.
- 854 Norbisrath, M., Pätsch, J., Dähnke, K., Sanders, T., Schulz, G., van Beusekom, J. E. E., and Thomas, H.: Metabolic
855 alkalinity release from large port facilities (Hamburg, Germany) and impact on coastal carbon storage,
856 *Biogeosciences*, 19, 5151–5165, <https://doi.org/10.5194/bg-19-5151-2022>, 2022.
- 857 Pätsch, J., Serna, A., Dähnke, K., Schlarbaum, T., Johannsen, A., and Emeis, K.-C.: Nitrogen cycling in the
858 German Bight (SE North Sea) — Clues from modelling stable nitrogen isotopes, *Cont. Shelf Res.*, 30, 203–213,
859 <https://doi.org/10.1016/j.csr.2009.11.003>, 2010.
- 860 Pind, A., Risgaard-Petersen, N., and Revsbech, N. P.: Denitrification and microphytobenthic NO₃⁻ consumption
861 in a Danish lowland stream: diurnal and seasonal variation, *Aquat. Microb. Ecol.*, 12, 275–284,
862 <https://doi.org/10.3354/ame012275>, 1997.
- 863 Quick, A. M., Reeder, W. J., Farrell, T. B., Tonina, D., Feris, K. P., and Benner, S. G.: Nitrous oxide from streams
864 and rivers: A review of primary biogeochemical pathways and environmental variables, *Earth-Sci. Rev.*, 191, 224–
865 262, <https://doi.org/10.1016/j.earscirev.2019.02.021>, 2019.
- 866 Quiel, K., Becker, A., Kirchesch, V., Schöl, A., and Fischer, H.: Influence of global change on phytoplankton and
867 nutrient cycling in the Elbe River, *Reg. Environ. Change*, 11, 405–421, <https://doi.org/10.1007/s10113-010-0152-2>, 2011.
- 869 The R Stats Package, Version 4.0.2:
870 <https://www.rdocumentation.org/packages/stats/versions/3.6.2/topics/prcomp>, last access: 29 January 2021.
- 871 Radach, G. and Pätsch, J.: Variability of continental riverine freshwater and nutrient inputs into the North Sea for
872 the years 1977–2000 and its consequences for the assessment of eutrophication, *Estuaries Coasts*, 30, 66–81,
873 <https://doi.org/10.1007/BF02782968>, 2007.

- 874 Reading, M. J., Tait, D. R., Maher, D. T., Jeffrey, L. C., Looman, A., Holloway, C., Shishaye, H. A., Barron, S.,
875 and Santos, I. R.: Land use drives nitrous oxide dynamics in estuaries on regional and global scales, *Limnol.*
876 *Oceanogr.*, 65, 1903–1920, <https://doi.org/10.1002/lno.11426>, 2020.
- 877 Redfield, A. C., Ketchum, B. H., and Richards, F. A.: The influence of organisms on the composition of sea-water,
878 *Compos. Seawater Comp. Descr. Oceanogr. Sea Ideas Obs. Prog. Study Seas*, 2, 26–77, 1963.
- 879 Rewrie, L. C. V., Voynova, Y. G., van Beusekom, J. E. E., Sanders, T., Körtzinger, A., Brix, H., Ollesch, G., and
880 Baschek, B.: Significant shifts in inorganic carbon and ecosystem state in a temperate estuary (1985 - 2018),
881 *Limnol. Oceanogr.*, submitted.
- 882 Rhee, T. S.: The process of air -water gas exchange and its application, Texas A&M University, College Station,
883 2000.
- 884 Rhee, T. S., Kettle, A. J., and Andreae, M. O.: Methane and nitrous oxide emissions from the ocean: A
885 reassessment using basin-wide observations in the Atlantic, *J. Geophys. Res. Atmospheres*, 114, D12304,
886 <https://doi.org/10.1029/2008JD011662>, 2009.
- 887 Robinson, A. D., Nedwell, D. B., Harrison, R. M., and Ogilvie, B. G.: Hypernutrified estuaries as sources of N 2
888 O emission to the atmosphere: the estuary of the River Colne, Essex, UK, *Mar. Ecol. Prog. Ser.*, 164, 59–71,
889 <https://doi.org/10.3354/meps164059>, 1998.
- 890 Rosenhagen, G., Schatzmann, M., and Schrön, A.: Das Klima der Metropolregion auf Grundlage meteorologischer
891 Messungen und Beobachtungen, in: *Klimabericht für die Metropolregion Hamburg*, edited by: von Storch, H. and
892 Claussen, M., Springer, Berlin, Heidelberg, 19–59, https://doi.org/10.1007/978-3-642-16035-6_2, 2011.
- 893 Rosentreter, J. A., Wells, N. S., Ulseth, A. J., and Eyre, B. D.: Divergent Gas Transfer Velocities of CO₂, CH₄,
894 and N₂O Over Spatial and Temporal Gradients in a Subtropical Estuary, *J. Geophys. Res. Biogeosciences*, 126,
895 e2021JG006270, <https://doi.org/10.1029/2021JG006270>, 2021.
- 896 Sanders, T., Schöl, A., and Dähnke, K.: Hot Spots of Nitrification in the Elbe Estuary and Their Impact on Nitrate
897 Regeneration, *Estuaries Coasts*, 41, 128–138, <https://doi.org/10.1007/s12237-017-0264-8>, 2018.
- 898 Scharfe, M., Callies, U., Blöcker, G., Petersen, W., and Schroeder, F.: A simple Lagrangian model to simulate
899 temporal variability of algae in the Elbe River, *Ecol. Model.*, 220, 2173–2186,
900 <https://doi.org/10.1016/j.ecolmodel.2009.04.048>, 2009.
- 901 Schoer, J. H.: Determination of the origin of suspended matter and sediments in the Elbe estuary using natural
902 tracers, *Estuaries*, 13, 161–172, <https://doi.org/10.2307/1351585>, 1990.
- 903 Schöl, A., Hein, B., Wyrwa, J., and Kirchesch, V.: Modelling Water Quality in the Elbe and its Estuary – Large
904 Scale and Long Term Applications with Focus on the Oxygen Budget of the Estuary, *Küste*, 203–232, 2014.
- 905 Schroeder, F.: Water quality in the Elbe estuary: Significance of different processes for the oxygen deficit at
906 Hamburg, *Environ. Model. Assess.*, 2, 73–82, <https://doi.org/10.1023/A:1019032504922>, 1997.
- 907 Sharma, N., Flynn, E. D., Catalano, J. G., and Giammar, D. E.: Copper availability governs nitrous oxide
908 accumulation in wetland soils and stream sediments, *Geochim. Cosmochim. Acta*, 327, 96–115,
909 <https://doi.org/10.1016/j.gca.2022.04.019>, 2022.
- 910 Siedler, G. and Peters, H.: Properties of sea water, Physical properties, in: *Oceanography*, vol. V/3a, edited by:
911 Sündermann, J., Springer, Berlin, Germany, 233–264, 1986.
- 912 Silvennoinen, H., Hietanen, S., Liikanen, A., Stange, C. F., Russow, R., Kuparinen, J., and Martikainen, P. J.:
913 Denitrification in the River Estuaries of the Northern Baltic Sea, *AMBIO J. Hum. Environ.*, 36, 134–140,
914 [https://doi.org/10.1579/0044-7447\(2007\)36\[134:DITREO\]2.0.CO;2](https://doi.org/10.1579/0044-7447(2007)36[134:DITREO]2.0.CO;2), 2007.
- 915 Sommerfield, C. K. and Wong, K.-C.: Mechanisms of sediment flux and turbidity maintenance in the Delaware
916 Estuary, *J. Geophys. Res. Oceans*, 116, C01005, <https://doi.org/10.1029/2010JC006462>, 2011.

- 917 Tang, W., Tracey, J. C., Carroll, J., Wallace, E., Lee, J. A., Nathan, L., Sun, X., Jayakumar, A., and Ward, B. B.:
 918 Nitrous oxide production in the Chesapeake Bay, *Limnol. Oceanogr.*, 67, 2101–2116,
 919 <https://doi.org/10.1002/lno.12191>, 2022.
- 920 Tian, H., Xu, R., Canadell, J. G., Thompson, R. L., Winiwarter, W., Suntharalingam, P., Davidson, E. A., Ciais,
 921 P., Jackson, R. B., Janssens-Maenhout, G., Prather, M. J., Regnier, P., Pan, N., Pan, S., Peters, G. P., Shi, H.,
 922 Tubiello, F. N., Zaehle, S., Zhou, F., Arneeth, A., Battaglia, G., Berthet, S., Bopp, L., Bouwman, A. F., Buitenhuis,
 923 E. T., Chang, J., Chipperfield, M. P., Dangal, S. R. S., Dlugokencky, E., Elkins, J. W., Eyre, B. D., Fu, B., Hall,
 924 B., Ito, A., Joos, F., Krummel, P. B., Landolfi, A., Laruelle, G. G., Lauerwald, R., Li, W., Lienert, S., Maavara,
 925 T., MacLeod, M., Millet, D. B., Olin, S., Patra, P. K., Prinn, R. G., Raymond, P. A., Ruiz, D. J., van der Werf, G.
 926 R., Vuichard, N., Wang, J., Weiss, R. F., Wells, K. C., Wilson, C., Yang, J., and Yao, Y.: A comprehensive
 927 quantification of global nitrous oxide sources and sinks, *Nature*, 586, 248–256, <https://doi.org/10.1038/s41586-020-2780-0>, 2020.
- 929 US EPA, ~~©~~: Volunteer Estuary Monitoring: A Methods Manual, United States Environmental Protection Agency
 930 (EPA), 2006.
- 931 Walter, S., Bange, H. W., and Wallace, D. W. R.: Nitrous oxide in the surface layer of the tropical North Atlantic
 932 Ocean along a west to east transect, *Geophys. Res. Lett.*, 31, L23S07, <https://doi.org/10.1029/2004GL019937>,
 933 2004.
- 934 Wanninkhof, R.: Relationship between wind speed and gas exchange over the ocean, *J. Geophys. Res. Oceans*, 97,
 935 7373–7382, <https://doi.org/10.1029/92JC00188>, 1992.
- 936 Weiss, R. F.: The solubility of nitrogen, oxygen and argon in water and seawater, *Deep Sea Res. Oceanogr. Abstr.*,
 937 17, 721–735, [https://doi.org/10.1016/0011-7471\(70\)90037-9](https://doi.org/10.1016/0011-7471(70)90037-9), 1970.
- 938 Weiss, R. F. and Price, B. A.: Nitrous oxide solubility in water and seawater, *Mar. Chem.*, 8, 347–359,
 939 [https://doi.org/10.1016/0304-4203\(80\)90024-9](https://doi.org/10.1016/0304-4203(80)90024-9), 1980.
- 940 Wells, N. S., Maher, D. T., Erler, D. V., Hipsey, M., Rosentreter, J. A., and Eyre, B. D.: Estuaries as Sources and
 941 Sinks of N₂O Across a Land Use Gradient in Subtropical Australia, *Glob. Biogeochem. Cycles*, 32, 877–894,
 942 <https://doi.org/10.1029/2017GB005826>, 2018.
- 943 Wertz, S., Goyer, C., Burton, D. L., Zebarth, B. J., and Chantigny, M. H.: Processes contributing to nitrite
 944 accumulation and concomitant N₂O emissions in frozen soils, *Soil Biol. Biochem.*, 126, 31–39,
 945 <https://doi.org/10.1016/j.soilbio.2018.08.001>, 2018.
- 946 de Wilde, H. P. and de Bie, M. J.: Nitrous oxide in the Schelde estuary: production by nitrification and emission
 947 to the atmosphere, *Mar. Chem.*, 69, 203–216, [https://doi.org/10.1016/S0304-4203\(99\)00106-1](https://doi.org/10.1016/S0304-4203(99)00106-1), 2000.
- 948 Winterwerp, J. C. and Wang, Z. B.: Man-induced regime shifts in small estuaries—I: theory, *Ocean Dyn.*, 63,
 949 1279–1292, <https://doi.org/10.1007/s10236-013-0662-9>, 2013.
- 950 WMO: Scientific Assessment of Ozone Depletion: 2018, World Meteorological Organization, Geneva,
 951 Switzerland, 2018.
- 952 Wolfstein, K. and Kies, L.: Composition of suspended particulate matter in the Elbe estuary: Implications for
 953 biological and transportation processes, *Dtsch. Hydrogr. Z.*, 51, 453–463, <https://doi.org/10.1007/BF02764166>,
 954 1999.
- 955 Wrage, N., Velthof, G. L., van Beusichem, M. L., and Oenema, O.: The role of nitrifier denitrification in the
 956 production of nitrous oxide, *Soil Biol. Biochem.*, 33, 1723–1732, [https://doi.org/10.1016/S0038-0717\(01\)00096-7](https://doi.org/10.1016/S0038-0717(01)00096-7), 2001.
- 958 Zander, F., Heimovaara, T., and Gebert, J.: Spatial variability of organic matter degradability in tidal Elbe
 959 sediments, *J. Soils Sediments*, 20, 2573–2587, <https://doi.org/10.1007/s11368-020-02569-4>, 2020.
- 960 Zander, F., Groengroeft, A., Eschenbach, A., Heimovaara, T. J., and Gebert, J.: Organic matter pools in sediments
 961 of the tidal Elbe river, *Limnologica*, 96, 125997, <https://doi.org/10.1016/j.limno.2022.125997>, 2022.

962 ZDM: Abfluss - Neu Darchau, edited by: Wasserstraßen- und Schifffahrtsamt Elbe, 2022.